Inorganic Chemistry

Article

pubs.acs.org/IC

Rational Design of Superoxide Dismutase (SOD) Mimics: The Evaluation of the Therapeutic Potential of New Cationic Mn Porphyrins with Linear and Cyclic Substituents

Artak Tovmasyan,[†] Sebastian Carballal,[§] Robert Ghazaryan,[∥] Lida Melikyan,[∥] Tin Weitner,[†] Clarissa G. C. Maia,[⊥] Julio S. Reboucas,[⊥] Rafael Radi,[§] Ivan Spasojevic,[‡] Ludmil Benov,[#] and Ines Batinic-Haberle*,[†]

[†]Departments of Radiation Oncology and [‡]Medicine, Duke University Medical Center, Research Drive, 281b MSRB I, Durham, North Carolina 27710, United States

[§]Departamento de Bioquímica and Center for Free Radical and Biomedical Research, Facultad de Medicina, Universidad de la República, Montevideo, Uruguay

[∥]Department of Organic Chemistry, Faculty of Pharmacy, Yerevan State Medical University, Yerevan, Armenia

[⊥]Departamento de Quimica, CCEN, Universidade Federal de Paraiba, Joao Pessoa, PB 58051-900, Brazil

[#]Department of Biochemistry, Faculty of Medicine, Kuwait University, Kuwait City, Kuwait

Supporting Information

ABSTRACT: Our goal herein has been to gain further insight into the parameters which control porphyrin therapeutic potential. Mn porphyrins (MnTnOct-2-PyP^{5+}, MnTnHex-OE-2-PyP^{5+}, MnTE-2-PyPhP^{5+}, and MnTPhE-2-PyP^{5+}) that bear the same positive charge and same number of carbon atoms at *meso* positions of porphyrin core were explored. The carbon atoms of their *meso* substituents are organized to form either linear or cyclic structures of vastly different redox properties, bulkiness, and lipophilicities. These Mn porphyrins were compared to frequently studied compounds, MnTE-2-PyP^{5+}, MnTE-3-PyP^{5+}, and MnTBAP^{3-}. All Mn(III) porphyrins (MnPs) have metal-centered reduction potential, $E_{1/2}$ for Mn^{III}P/Mn^{II}P redox couple, ranging from −194 to +340 mV versus NHE, log $k_{cat}(O_2^{\bullet-})$ from 3.16 to 7.92, and log $k_{red}(ONOO^-)$ from 5.02 to 7.53. The lipophilicity, expressed as partition between n-octanol and water, log P_{OW}, was in the range −1.67 to −7.67. The therapeutic potential of MnPs was assessed via: (i) *in vitro* ability to prevent spontaneous lipid peroxidation in rat brain homogenate as assessed by malondialdehyde levels; (ii) *in vivo* $O_2^{\bullet-}$ specific assay to measure the efficacy in protecting the aerobic growth of SOD-deficient *Saccharomyces cerevisiae*; and (iii) aqueous solution chemistry to measure the reactivity toward major *in vivo* endogenous antioxidant, ascorbate. Under the conditions of lipid peroxidation assay, the transport across the cellular membranes, and in turn shape and size of molecule, played no significant role. Those MnPs of $E_{1/2} \sim +300$ mV were the most efficacious, significantly inhibiting lipid peroxidation in 0.5−10 μM range. At up to 200 μM, MnTBAP^{3-} ($E_{1/2} = -194$ mV vs NHE) failed to inhibit lipid peroxidation, while MnTE-2-PyPhP^{5+} with 129 mV more positive $E_{1/2}$ (−65 mV vs NHE) was fully efficacious at 50 μM. The $E_{1/2}$ of Mn^{III}P/Mn^{II}P redox couple is proportional to the log $k_{cat}(O_2^{\bullet-})$, *i.e.*, the SOD-like activity of MnPs. It is further proportional to $k_{red}(ONOO^-)$ and the ability of MnPs to prevent lipid peroxidation. In turn, the inhibition of lipid peroxidation by MnPs is also proportional to their SOD-like activity. In an *in vivo S. cerevisiae* assay, however, while $E_{1/2}$ predominates, lipophilicity significantly affects the efficacy of MnPs. MnPs of similar log P_{OW} and $E_{1/2}$, that have linear alkyl or alkoxyalkyl pyridyl substituents, distribute more easily within a cell and in turn provide higher protection to *S. cerevisiae* in comparison to MnP with bulky cyclic substituents. The bell-shape curve, with MnTE-2-PyP^{5+} exhibiting the highest ability to catalyze ascorbate oxidation, has been established and discussed. Our data support the notion that the SOD-like activity of MnPs parallels their therapeutic potential, though species other than $O_2^{\bullet-}$, such as peroxynitrite, H_2O_2, lipid reactive species, and cellular reductants, may be involved in their mode(s) of action(s).

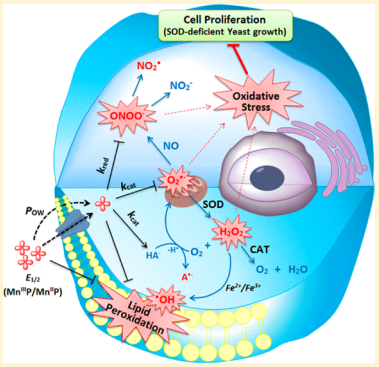

INTRODUCTION

Our continuous goal has been to learn how to improve the therapeutic potential of porphyrin-based SOD mimics for the treatment of disorders with perturbed cellular redox environment, commonly described as oxidative stress. While maintaining the most appropriate thermodynamics and kinetics for SOD-like activity, the efforts have recently been directed toward the increase in the biodistribution of SOD mimics and decrease in their toxicity. The structure−activity relationship

Received: June 9, 2014
Published: October 21, 2014

   dx.doi.org/10.1021/ic501329p | *Inorg. Chem.* 2014, 53, 11467−11483

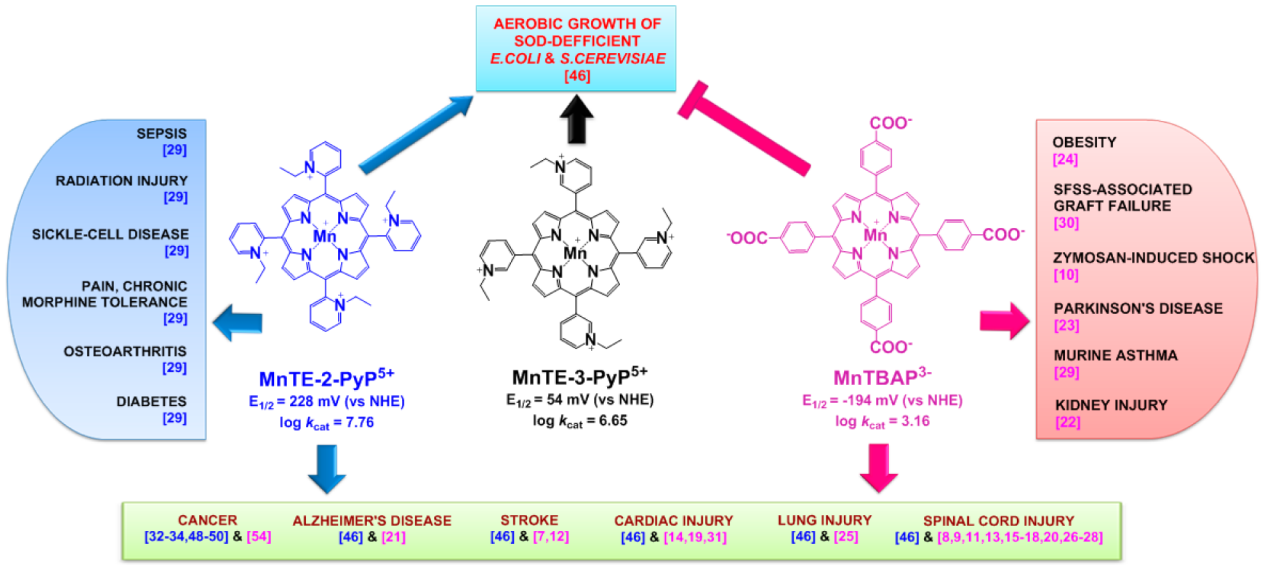

Figure 1. Structures of $MnTBAP^{3-}$,[18−42] and *ortho* (2) and *meta* (3) isomers, MnTE-2(and 3)-PyP^{5+}.[43−68] Also listed are their *in vivo* efficacy studies.

(SAR), which has guided us in our efforts to improve the drug quality,[1,2] correlates the thermodynamic (metal-centered reduction potential, $E_{1/2}$, for $Mn^{III}P/Mn^{II}P$ redox couple) and kinetic properties of Mn(III) porphyrins (MnPs), log $k_{cat}(O_2^{\bullet-})$ ($O_2^{\bullet-}$, superoxide). The $k_{cat}(O_2^{\bullet-})$ describes the ability of MnP to catalyze $O_2^{\bullet-}$ dismutation to O_2 and H_2O_2. SAR is universally valid, not only for metalloporphyrins but for other redox-active drugs also.[2,3] Further, $k_{cat}(O_2^{\bullet-})$ parallels the ability of MnPs to reduce peroxynitrite, described by the rate constant for $ONOO^-$ (peroxynitrite) reduction, $k_{red}(ONOO^-)$.[4] Both properties are controlled by the electron-deficiency of a metal site which favors exchanging electrons with $O_2^{\bullet-}$ (reducing and oxidizing it during dismutation process) and binding of electron-rich $ONOO^-$ with its subsequent reduction to either $^{\bullet}NO_2$ (one-electronically) or NO_2^- (two-electronically).[4−6] We have further shown that such property of the metal site also favors reactions with other electron-rich nucleophiles such as ClO^- (deprotonated hypochlorite),[7] HO_2^- (a deprotonated reactive species of H_2O_2), lipid radicals,[8,9] $CO_3^{\bullet-}$,[4] ascorbate, HA^- (monodeprotonated ascorbic acid), and deprotonated thiols, RS^-.[10−12] The reaction of MnPs with simple and protein thiols as well as with ascorbate coupled to peroxide production seems to be heavily involved in their mechanism(s) of action(s).[2,10]

With the goal to enhance the biodistribution of MnPs, we modified the original structure of MnTE-2-PyP^{5+} (AEOL10113, Mn(III) *meso*-tetrakis(*N*-ethylpyridinium-2-yl)porphyrin) and synthesized a first generation of lipophilic analogs, via lengthening the alkyl chains of MnTE-2-PyP^{5+} to MnTnOct-2-PyP^{5+} (Mn(III) *meso*-tetrakis(*N*-n-octylpyridinium-2-yl)-porphyrin).[13] MnTnHex-2-PyP^{5+} (Mn(III) *meso*-tetrakis(*N*-*n*-hexylpyridinium-2-yl)porphyrin) has been a well-explored lipophilic analog with much higher brain and mitochondrial distribution than MnTE-2-PyP^{5+}.[14,15] Yet, its toxicity at higher concentration and prolonged administration may limit its use. We thus designed and characterized MnTnBuOE-2-PyP^{5+} (BMX-001; Mn(III) *meso*-tetrakis(*N*-(2′-*n*-butoxyethyl)-pyridinium-2-yl)porphyrin), which has 4−5-fold reduced toxicity relative to MnTnHex-2-PyP^{5+}, while lipophilicity and redox-activity have not been compromised.[16]

Herein we continued with the rational design of MnPs. New Mn porphyrins were synthesized and compared to MnTnOct-2-PyP^{5+} and several other compounds (Figures 1 and 2) mostly studied by us and others, MnTE-2-PyP^{5+}, MnTE-3-PyP^{5+} (Mn(III) *meso*-tetrakis(*N*-ethylpyridinium-3-yl)porphyrin), and $MnTBAP^{3-}$ (Mn(III) *meso*-tetrakis(4-carboxylatophenyl)-porphyrin).[2,17] While of entirely different redox properties, both an SOD mimic, MnTE-2-PyP^{5+}, and a non-SOD mimic, $MnTBAP^{3-}$, reportedly exhibit beneficial effects in *in vitro* and *in vivo* models of numerous oxidative stress-related disorders, such as stroke, cancer, lung diseases, radiation injuries, spinal cord injury, Alzheimer disease, cardiac injuries, pain, and morphine tolerance and autoimmune diseases, some of which are shown in Figure 1.[18−68]

We have been puzzled with the therapeutic efficacy of the $MnTBAP^{3-}$ [see also Results and Discussion]. On the basis of our present knowledge, this compound has inferior redox properties ($E_{1/2}$ = −194 mV vs NHE), relative to MnTE-2-PyP^{5+} ($E_{1/2}$ = +228 mV vs NHE) and thus does not favor interactions with biological targets. Most of the reactive species are anionic and would disfavor interacting with anionic $MnTBAP^{3-}$ on electrostatic grounds.[69] Still strongly oxidizing species such as $ONOO^-$ and $CO_3^{\bullet-}$ are able to oxidize it.[4,5,9] Despite claims,[70] $MnTBAP^{3-}$ is neither reactive toward $O_2^{\bullet-}$ nor to H_2O_2. Recent data indicate that its RNS-related chemistry may account for its biological effects;[71] the neutrality of $^{\bullet}NO$ or HNO would work in favor of such reactions.[72] Finally, its negative charge would not facilitate its transport across anionic phospholipid membranes. The fact that impure preparations of $MnTBAP^{3-}$, provided by several commercial sources, were often used without prior characterization and purification has complicated things further.[69,73] Still the abundance of published data, including a few of our studies, indicates that under certain conditions $MnTBAP^{3-}$ is efficacious.[5,9,18−42,72] Recently, a manuscript was published where PEG-ylated amid of $MnTBAP^{3-}$ was synthesized and characterized.[74] Such derivatization removed the unfavorable electron-donating effect of COO^- groups upon Mn site. In turn, the $E_{1/2}$ is nearly 200 mV more positive relative to $MnTBAP^{3-}$. Along with the improved electrostatics, this modification increased log $k_{cat}(O_2^{\bullet-})$ from 3.16 to 5.6. The

dx.doi.org/10.1021/ic501329p | *Inorg. Chem.* 2014, 53, 11467−11483

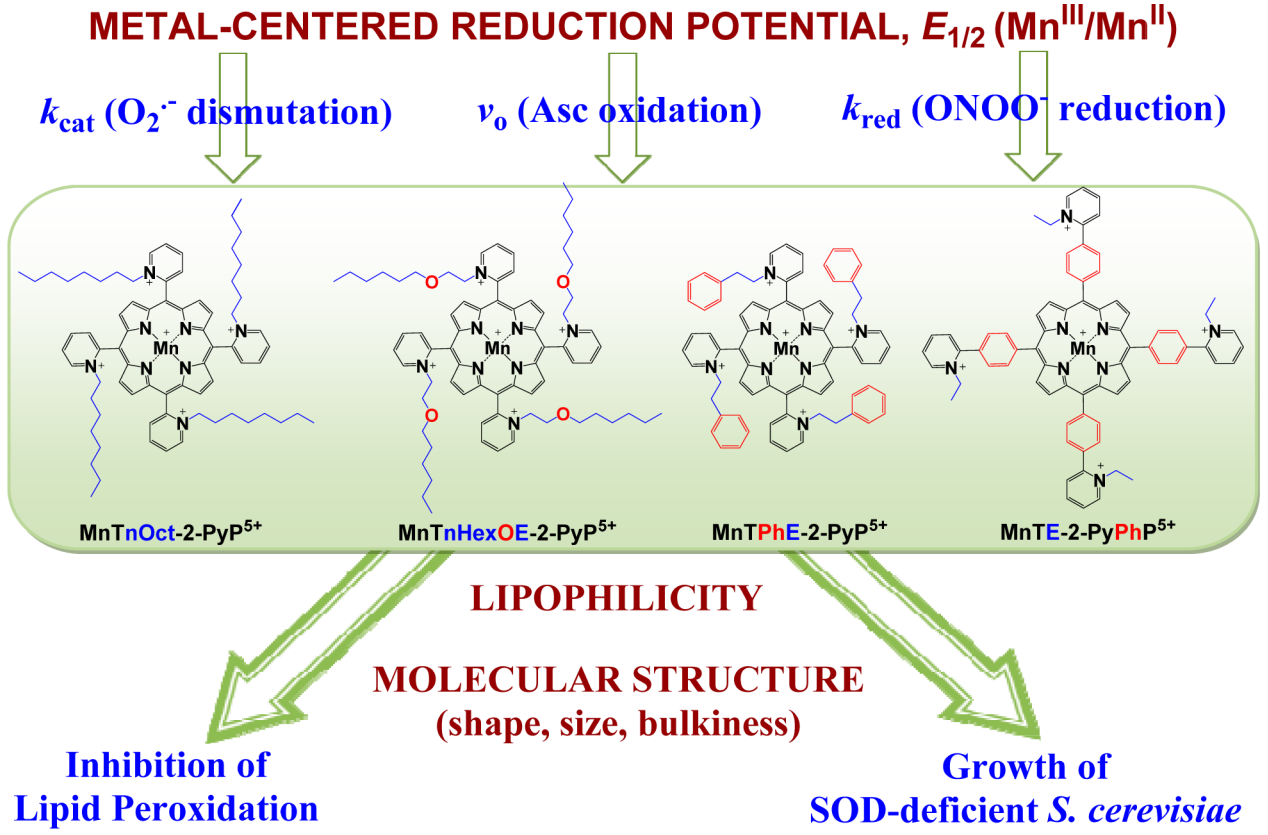

Figure 2. Impact of structural features of MnTnOct-2-PyP^{5+} and three new Mn porphyrins (MnPs) on their *in vitro* and *in vivo* therapeutic potential. The figure illustrates which properties of MnPs were studied herein with a goal to (i) further our knowledge on their impact on the therapeutic potential of redox-active drugs, and in turn (ii) facilitate drug development. Metal-centered reduction potential, $E_{1/2}$ of $Mn^{III}P/Mn^{II}P$, controls the rate constant for the catalysis of $O_2^{\bullet-}$, $k_{cat}(O_2^{\bullet-})$, rate constant for the peroxynitrite reduction, $k_{red}(ONOO^-)$, as well as the ability of MnP to catalyze ascorbate oxidation to ascorbyl radical A$^{\bullet}$. The *in vitro* consequences of appropriate thermodynamics were also witnessed in the lipid peroxidation of rat brain homogenate. This is so because the reduction of highly reactive species, such as $ONOO^-$ and lipid reactive species, involves their binding to Mn site in the first step. Binding is controlled by electron-deficiency of porphyrin and its Mn site and could be best described by the protonation equilibria of porphyrin inner pyrrolic nitrogens[76] and axial waters,[4] which in turn control the $E_{1/2}$ of $Mn^{III}P/Mn^{II}P$. With $E_{1/2}$ value beyond 0 mV vs NHE, the fair deficiency in electron density of the metal site is indicated which in turn suggests the high affinity of Mn toward binding of an electron-rich ligand, such as $ONOO^-$ or lipid reactive species. Ligand binding is followed by $Mn^{III}P$ oxidation to $O{=}Mn^{IV}P$. Therefore, the $E_{1/2}$ of $Mn^{III}P/Mn^{II}P$ redox couple correlates well with rates of reactions involving the $O{=}Mn^{IV}P/Mn^{III}P$ redox couple. The $E_{1/2}$ of $O{=}Mn^{IV}P/Mn^{III}P$ redox couple is similar for a variety of different Mn and Fe porphyrins, implying that the ligand (such as $ONOO^-$) binding is a rate-limiting step in metal oxidation and ligand reduction (see also Results and Discussion). The other major property that controls the therapeutic potential of MnP is its lipophilicity, and it was herein explored in aerobic growth of SOD-deficient yeast *S. cerevisiae*.

impact of such derivatization agrees well with our data on the contribution of electrostatics in $O_2^{\bullet-}$ dismutation.[75] In order to gain further insight into the possible therapeutic effects of $MnTBAP^{3-}$, we have used it in all studies performed herein.

From a therapeutic point of view, if the drug is efficacious it may not quite matter what exactly it is doing *in vivo*. This fact may not preclude its clinical development. Yet, understanding the drug biology matters largely if it is used to clarify the metabolic pathways involved in certain models of diseases. Importantly, it provides us with valuable feedback for improving the design of not only MnPs, but also other redox-active drugs. With this in mind, we are continuing here with rational design of redox-active SOD mimics. The compounds of the same charge and same number of carbon atoms, organized in different ways, are synthesized and characterized as indicated in Figure 2. These MnPs have different redox properties, bulkiness (size and shape), and lipophilicities. They were tested in an *in vitro* model of lipid peroxidation and in an *in vivo* $O_2^{\bullet-}$-specific model of aerobic growth of *S. cerevisiae*. This model has over the years unambiguously identified the clinical drug candidates.[2,67] Upon entering the cell, MnPs encounter ascorbate due to its high *in vivo* abundance. Thus, cycling with ascorbate seems to be heavily involved in their actions. Moreover, the combination of ascorbate and MnP holds a promising therapeutic modality for cancer treatment.[2,77,78] Therefore, the reactivity of MnPs toward ascorbate has been explored also.

EXPERIMENTAL SECTION

General. *meso*-Tetrakis(2-*N*-pyridyl)porphyrin (H_2T-2-PyP) and *meso*-tetrakis(3-*N*-pyridyl)porphyrin (H_2T-3-PyP) were purchased from Frontier Scientific. Ethyl *p*-toluenesulfonate (98%) was from Sigma-Aldrich. The *n*-octyl *p*-toluenesulfonate and methyl-tri-n-octylammonium chloride (>95%) were from TCI America. $MnCl_2 \cdot 4H_2O$ (99.7%) was supplied by J. T. Baker, $FeCl_2$ (98%) was from Sigma-Aldrich, and NH_4PF_6 (99.99%) was from GFS chemicals. Anhydrous diethyl ether and acetone were from EMD chemicals, while dichloromethane, chloroform, acetonitrile, EDTA, and KNO_3 were purchased from Mallinckrodt. Anhydrous *N*,*N*-dimethylformamide (DMF) of 99.8% purity (kept over 4-Å molecular sieves) and plastic-backed silica gel TLC plates (Z122777-25EA) were from Sigma-

dx.doi.org/10.1021/ic501329p | *Inorg. Chem.* 2014, 53, 11467−11483

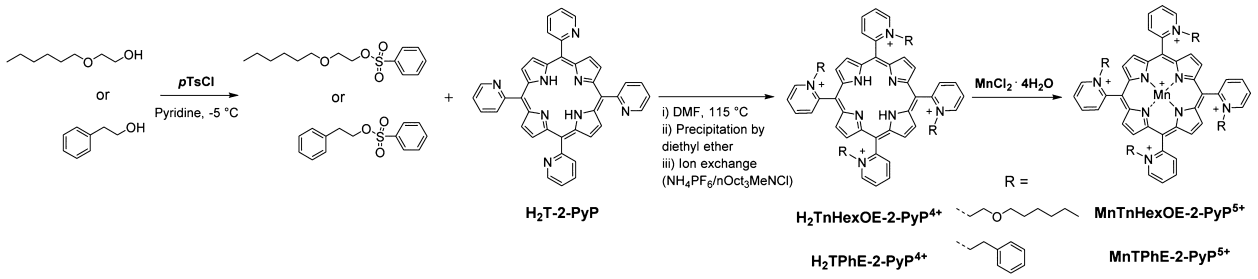

Figure 3. Synthesis of new porphyrinic ligands, H_2TPhE-2-PyPCl_4 and H_2TnHexOE-2-PyPCl_4, and their Mn complexes, MnTPhE-2-PyPCl_5 and MnTnHexOE-2-PyPCl_5.

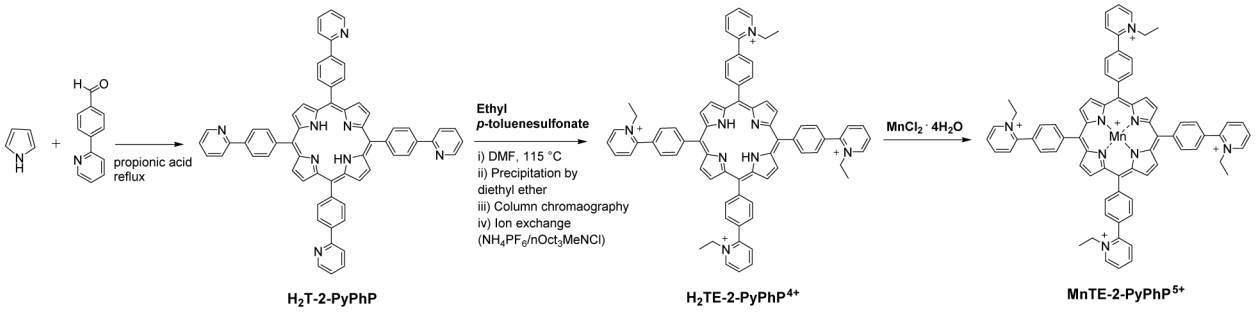

Figure 4. Synthesis of new porphyrinic ligands, H_2T-2-PyPhP and H_2TE-2-PyPhPCl_4, and a Mn complex, MnTE-2-PyPhPCl_5.

Aldrich. Xanthine, equine ferricytochrome *c* (lot 7752), and (+)-sodium L-ascorbate (>98%) were from Sigma, whereas xanthine oxidase was prepared by R. Wiley.[1] Triethylamine (Et_3N) of >99.5% purity was obtained from Thermo Scientific Pierce. All chemicals were used as received without further purification. The ^{1}H NMR spectra were recorded on a spectrometer "Mercury Varian 300" with deuterated chloroform as solvent.

Synthesis of *meso*-Tetrakis(*N*-substituted pyridinium-2-yl)-porphyrins. The general synthetic procedure for *meso*-tetrakis(*N*-substituted pyridinium-2-yl)porphyrins and their Mn complexes is shown in Figure 3. The synthesis, isolation, purification, and characterization of Mn porphyrins, MnTE-2-PyPCl_5, MnTE-3-PyPCl_5, MnTnOct-2-PyPCl_5, and MnTBAP^{3-}, were performed as described earlier.[76,79] The appropriate tosylates, phenylethyl *p*-toluenesulfonate and 2-n-hexoxyethyl *p*-toluenesulfonate, were obtained, purified, and characterized according to the methods earlier reported for analogous compounds.[80] The synthesis of new porphyrinic ligands H_2TPhE-2-PyPCl_4 (*meso*-tetrakis(*N*-(2′-phenylethyl)pyridinium-2-yl)porphyrin tetrachloride) and H_2TnHexOE-2-PyPCl_4 (*meso*-tetrakis(*N*-(2′-n-hexoxyethyl)-pyridinium-2-yl)porphyrin tetrachloride)) and their Mn complexes is illustrated in Figure 3.

H_2TPhE-2-PyPCl_4, meso-Tetrakis(N-(2′-phenylethyl)pyridinium-2-yl)porphyrin Tetrachloride. H_2T-2-PyP (100 mg; 0.162 mmol) was dissolved in 4.6 mL of DMF preheated for 10 min at 115 °C. To the resulting solution was added the 9 g (0.032 mol) of phenylethyl *p*-toluenesulfonate. The course of *N*-quaternization was followed by thin-layer chromatography (TLC) on silica gel plates using acetonitrile/KNO_3(sat)/water = 8/1/1 as a mobile phase. Also, methanol/chloroform (1/4) solvent system has been used to monitor the reaction progress. The reaction was completed within 25 h. Porphyrin was precipitated from the reaction mixture by diethyl ether, filtered, and washed with diethyl ether (5 × 30 mL). The porphyrin tosylate was then dissolved in 100 mL of hot water and precipitated as the PF_6^- salt with saturated aqueous solution of NH_4PF_6. The precipitate was thoroughly washed with diethyl ether. The dried precipitate was then dissolved in acetone, solution filtered and porphyrin precipitated from it as a chloride salt with saturated acetone solution of methyl-tri-n-octylammonium chloride. The precipitate was washed with acetone and dissolved in water. The double precipitation was repeated once again to ensure the highest purity of preparation. The porphyrin was dried in vacuum oven in the form of Cl^- salt. Yield (calculated based on elemental analysis): 180 mg (94.3%).

MnTPhE-2-PyPCl_5, Mn(III) meso-Tetrakis(N-(2′-phenylethyl)-pyridinium-2-yl)porphyrin Pentachloride. The pH of 40 mL aqueous solution of H_2TPhE-2-PyPCl_4 (50 mg) was adjusted to 10.9 (with 1 M NaOH), and a 20-fold molar excess of $MnCl_2{\cdot}4H_2O$ (0.847 mmol; 167.4 mg) was added into the solution at 25 °C while stirring. The pH of the solution dropped to 7.6. The stirring was continued at 100 °C for 3.5 h until metalation was completed. The course of metalation was followed on silica gel TLC plates using acetonitrile/KNO_3(sat)/water = 8/1/1 as a mobile phase. The pH of the solution was periodically adjusted to 7.2. Additionally, the course of metalation was monitored as a disappearance of porphyrin ligand fluorescence under UV light at ∼350 nm. The porphyrin solution was filtered first through coarse and then through fine filter paper. The MnP was precipitated as a PF_6^- salt with saturated aqueous solution of NH_4PF_6. The precipitate was thoroughly washed with diethyl ether. The dried precipitate was then dissolved in acetone, filtered, and precipitated as the chloride salt with saturated acetone solution of methyl-tri-n-octylammonium chloride. The precipitate was washed with acetone and dissolved in water. The double precipitation was repeated once again to ensure the highest purity of porphyrin and complete removal of free manganese species.

H_2TnHexOE-2-PyPCl_4, meso-Tetrakis(N-(2′-n-hexoxyethyl)-pyridinium-2-yl)porphyrin Tetrachloride. The synthesis was similar to the one described for H_2TPhE-2-PyPCl_4. Briefly, to a 70 mg portion of H_2T-2-PyP in 4 mL of DMF, preheated for ∼5 min at 115 °C, was added the 8.5 g of 2-n-hexoxyethyl *p*-toluenesulfonate (0.028 mol). The reaction was completed within 48 h. The porphyrin was isolated as described for H_2TPhE-2-PyPCl_4.

MnTnHexOE-2-PyPCl_5, Mn(III) meso-Tetrakis(N-(2′-n-hexoxyethyl)pyridinium-2-yl)porphyrin Pentachloride. The metalation was similar to the procedure described for the MnTPhE-2-PyPCl_5. Briefly, the pH of 80 mL of H_2TnHexOE-2-PyPCl_4 aqueous solution (100 mg, 0.078 mmol) was adjusted to 10.9, and a 40-fold excess of $MnCl_2$ (620 mg, 3.1 mmol) was added into the solution while stirring at 25 °C for 2.5 h. The porphyrin was isolated and purified in quantitative yield as described for MnTPhE-2-PyPCl_5.

Synthesis of *meso*-Tetrakis(phenyl-4-(2′-*N*-pyridyl))-porphyrins. Synthesis of new porphyrinic ligands H_2T-2-PyPhP (*meso*-tetrakis(phenyl-4-(2′-*N*-pyridyl))porphyrin), and H_2TE-2-PyPhPCl_4 (*meso*-tetrakis(phenyl-4-(*N*-ethylpyridinium-2′-yl))-

dx.doi.org/10.1021/ic501329p | *Inorg. Chem.* 2014, 53, 11467−11483

porphyrin tetrachloride), and MnTE-2-PyPhPCl$_5$ (Mn(III) *meso*-tetrakis(phenyl-4-(*N*-ethylpyridinium-2′-yl))porphyrin pentachloride) was performed as illustrated in Figure 4.

H$_2$T-2-PyPhP, meso-Tetrakis(phenyl-4-(2′-N-pyridyl))porphyrin. 4-(2-Pyridyl)benzaldehyde (5 g, 0.027 mol) was added to a boiling propionic acid (100 mL). Pyrrole (1.85 g, 0.027 mol) was added to the reaction mixture and was stirred for 45 min. The solution was stirred for another 2 h at room temperature and was left overnight in dark. The precipitate formed was filtered, washed with diluted aqueous solution of NaHCO$_3$, cold water, hot water, cold water and finally with small portions of methanol, and was left overnight to dry. The obtained violet crystals were dissolved in chloroform and were purified by column chromatography (absorbent, alumina; eluent, chloroform). The solvent was evaporated under reduced pressure, and the porphyrin was air-dried. Yield: 1.1 g (17.47%). H$_2$T-2-PyPhP porphyrin ($C_{64}H_{42}N_8$) M_r = 923.1. ^{1}H NMR (300 MHz; $CDCl_3$; Me_4Si) δ_H, ppm: −2.72 (2H, s, pyrrole-N*H*); 7.38 (4H, dd, *J* = 7.5, *J* = 4.8, pyridine-4-*H*); 7.94 (4H, dd, *J* = 8.0, *J* = 7.5, *J* = 1.8, pyridine-5-*H*); 8.16 (4H, d, *J* = 8.0, pyridine-6-*H*); 8.31−8.36 (8H, m, phenyl-*H*); 8.49−8.54 (8H, m, phenyl-*H*); 8.79 (4H, ddd, *J* = 4.8, *J* = 1.8, *J* = 0.9, pyridine-3-*H*); 8.91 (8H, s, *β*-pyrrole-*H*). Elemental Analysis H$_2$T-2-PyPhP·2.5H$_2$O, Anal. Calcd for $C_{72}H_{47}N_8O_{2.5}$: H, 4.89; C, 79.40; N, 11.57%. Found: H, 5.00; C, 79.36; N, 11.37%. UV−vis ($CHCl_3$): λ_{max}, nm (log ε) 252.5 (4.75), 275.3 (4.66), 373.9 (4.43), 422.5 (5.71), 517.5 (4.30), 553.8 (4.10), 592.1 (3.81), 648.6 (3.79).

H$_2$TE-2-PyPhPCl$_4$, meso-Tetrakis(phenyl-4-(N-ethylpyridinium-2′-yl))porphyrin Tetrachloride. H$_2$T-2-PyPhP (50 mg; 0.542 mmol) was dissolved in 4.5 mL of DMF at 115 °C, preheated for 20 min while purged with nitrogen. To the resulting solution was added 3.8 g (0.019 mol) of ethyl *p*-toluenesulfonate. The course of *N*-ethylation was followed on TLC silica gel plates using acetonitrile/KNO$_3$(sat)/water = 8/1/1 as a mobile phase. After 20 h of stirring, a new portion of 1.64 g of ethyl *p*-toluenesulfonate was added and stirred for another 26 h at 115 °C until reaction was completed. The *N*-quaternization with ethyl *p*-toluenesulfonate led to the formation of tetracationic ligand, H$_2$TE-2-PyPhP^{4+}. Interestingly, the reaction progressed very slowly when compared to the 3 h reaction time of *N*-ethylation of H$_2$T-2-PyP under similar conditions. Such a difference in reaction rates is due to the steric and electronic effects imposed by the coplanarity of phenyl and pyridyl moieties of H$_2$T-2-PyPhP. Due to the prolonged reaction time, additional spots appeared on TLC plate, and were separated by column chromatography. Though not fully characterized, these impurities are most likely the products of alkylation of inner pyrrolic nitrogens.

H$_2$TE-2-PyPhP^{4+} was precipated from the reaction mixture by diethyl ether, filtrated, and washed with diethyl ether (5 × 50 mL). It was isolated as a Cl^- salt as described above via two PF_6^-/Cl^- sequential precipitations. The solid was then chromatographed on column chromatography with 1/500 = Et_3N/(1/1/8 = KNO$_3$/saturated H$_2$O/acetonitrile) as a solvent system. Solvent was evaporated under reduced pressure and the porphyrin isolated after two PF_6^-/Cl^- sequential precipitations. The Cl^- salt was dried in a vacuum oven. Yield (calculated based on elemental analysis): 51 mg (80%).

MnTE-2-PyPhPCl$_5$, Mn(III) meso-Tetrakis(phenyl-4-(N-ethylpyridinium-2′-yl))porphyrin Pentachloride. The 40 mg portion of H$_2$TE-2-PyPhPCl$_4$ (0.34 mmol) was dissolved in 40 mL of water, and the pH of the resulting solution was adjusted to 11.7. A 40-fold excess of MnCl$_2$·4H$_2$O (1.35 mmol, 0.27 g) was added into the solution at 25 °C while stirring, and was accompanied by the pH drop to ∼8.5. The solution was then heated for another hour at 100 °C to allow for the completion of metalation. The course of reaction was followed on silica gel TLC plates using acetonitrile/KNO$_3$(sat)/water = 8/1/1 as a mobile phase. The isolation and purification of the MnTE-2-PyPhPCl$_5$ was done as described above for the *ortho* Mn pyridylporphyrins. The isolated yield was quantitative, 41 mg (95.3%).

Elemental Analysis. Elemental analyses of porphyrins and their Mn complexes were performed in duplicates with Atlantic MicroLab (Norcross, GA) and average values presented.

H$_2$TPhE-2-PyPCl$_4$·10H$_2$O. Anal. Calcd for $C_{72}H_{82}Cl_4N_8O_{10}$: H, 6.07; C, 63.53; N, 8.23; Cl, 10.42%. Found: H, 6.14; C, 63.29; N, 8.20; Cl, 10.17%.

MnTPhE-2-PyPCl$_5$·9H$_2$O. Anal. Calcd for $C_{72}H_{18}Cl_5MnN_8O_9$: H, 5.49; C, 60.41; N, 7.83; Cl, 12.38%. Found: H, 5.70; C, 60.37; N, 7.85; Cl, 12.11%.

H$_2$TnHexOE-2-PyPCl$_4$·8H$_2$O. Anal. Calcd for $C_{72}H_{110}Cl_4N_8O_{12}$: H, 7.8; C, 60.84; N, 7.88%. Found: H, 7.72; C, 60.56; N, 7.92%.

MnTnHexOE-2-PyPCl$_5$·8.5H$_2$O. Anal. Calcd for $C_{64}H_{94}Cl_5MnN_8O_9$: H, 7.23; C, 56.93; N, 7.38; Cl, 11.67%. Found: H, 7.05; C, 56.58; N, 7.68; Cl, 11.28%.

H$_2$TE-2-PyPhPCl$_4$·10.5H$_2$O·0.5KNO$_3$·2KCl. Anal. Calcd for $C_{72}H_{83}Cl_6MnN_8O_{12}K_{2.5}$: H, 5.30; C, 55.40; N, 7.63; Cl, 13.63%. Found: H, 5.40; C, 55.74; N, 7.66; Cl, 14.60%.

MnTE-2-PyPhPCl$_5$·10.5H$_2$O. Anal. Calcd for $C_{72}H_{81}Cl_5MnN_8O_{10.5}$: H, 5.60; C, 59.29; N, 7.68; Cl, 12.15%. Found: H, 5.48; C, 59.42; N, 7.50; Cl, 11.93%.

UV−Vis Spectroscopy. UV−vis spectra were recorded in water at room temperature on a UV-2501PC Shimadzu spectrophotometer with 0.5 nm resolution in 1 cm quartz cuvette (Table 1). The UV−vis spectra for new compounds are provided in Supporting Information (Figures S1−S3).

Table 1. Spectral Properties of Porphyrins and Their Mn Complexes

(metallo) porphyrin	λ_{max} nm (log ε)[a]
MnTBAP[b]	230.0 (4.93), 290.0 (4.49), 381.0 (4.84), 401.0 (4.84), 420.0 (sh, 4.70), 468.0 (5.04), 515.0 (3.92), 566.0 (4.16), 599.0 (4.07), 684.0 (sh, 3.23), 712.0 (sh, 3.20), 780.0 (3.24), 811.0 (sh, 3.17)
MnTE-2-PyPCl$_5$[b]	363.5 (4.68), 409.0 (4.32), 454.0 (5.14), 499.0 (3.75), 558.0 (4.08), 782.0 (3.26)
MnTE-3-PyPCl$_5$[b]	214.0 (4.77), 260.0 (4.60), 373.0 (4.74), 395.0 (4.78), 460.0 (5.19), 502.0 (3.85), 557.0 (4.16), 674.0 (3.25), 766.0 (3.37), 837.0 (2.40)
H$_2$TnHexOE-2-PyPCl$_4$	264.4 (4.38), 419.4 (5.35), 513.5 (4.27), 545.5 (3.64), 586.4 (3.86), 640 (3.43)
MnTnHexOE-2-PyPCl$_5$	212.5 (4.72), 261.7 (4.56), 365.4 (4.74), 411.4 (4.39), 455.5 (5.26), 561.1 (4.16), 786.5 (3.38)
H$_2$TPhE-2-PyPCl$_4$	263.2 (4.41), 419.4 (5.34), 514.6 (4.24), 585.6 (3.85), 638.6 (3.26)
MnTPhE-2-PyPCl$_5$	260.7 (4.60), 364.9 (4.72), 455.5 (5.27), 560.4 (4.17), 783.1 (3.41)
H$_2$TE-2-PyPhPCl$_4$	274.2 (4.62), 414.2 (5.77), 515.5 (4.29), 552.1 (3.95), 579.8 (3.88), 634.1 (3.64)
MnTE-2-PyPhPCl$_5$	273.1 (4.71), 378.7 (4.82), 400 (4.83), 466.3 (5.06), 514 (3.90), 562.5 (4.15), 597.1 (4.01), 773.8 (3.27)
MnTnOct-2-PyPCl$_5$[b]	364.0 (4.72), 414.0 (4.44), 454.5 (5.24), 500.5 (3.84), 559.5 (4.14), 781.0 (3.25)

[a]Spectra were recorded in water at room temperature unless otherwise noted. Molar absorption coefficients (M^{-1} cm^{-1}) were determined within 5% errors. λ_{max} (nm) were determined with errors inside ±0.5 nm. [b]Data are taken from ref 79.

Electrospray-Ionization Mass Spectrometry. Electrospray ionization mass spectrometric (ESI-MS) analyses were performed on Applied Biosystems MDS Sciex 3200 Q Trap LC/MS/MS spectrometer at Duke Comprehensive Cancer Center, Shared Resource PK Laboratories, as described elsewhere.[73,80,81] Samples of ∼1 μM concentrations were prepared in acetonitrile/H$_2$O mixture (1/1, v/v) containing 0.01% v/v heptafluorobutyric acid, and infused for 1 min at 10 μL/min into the spectrometer (curtain gas 20 V, ion spray voltage 3500 V, ion source 30 V, *T* = 300 °C, declustering potential 20 V, entrance potential 1 V, collision energy 5 V, gas N$_2$). Under given conditions, in the presence of ion-pairing heptafluorobutyrate anion ($HFBA^-$), no fragmentation was observed; the data relate to species originally present in solutions. The absence of peaks associated with partially alkylated and nonmetalated species unambiguously indicates

dx.doi.org/10.1021/ic501329p | Inorg. Chem. 2014, 53, 11467−11483

Table 2. Electrospray Ionization Mass Spectrometry (ESI-MS) Data for New Porphyrins, H_2P, and their Mn(III) Complexes[a]

species[a]	m/z [found (calcd)]					
	H_2TnHexOE-2-PyP^{4+}	MnTnHexOE-2-PyP^{5+}	H_2TPhE-2-PyP^{4+}	MnTPhE-2-PyP^{5+}	H_2TE-2-PyPhP^{4+}	MnTE-2-PyPhP^{5+}
$[P^{n+} + HFBA^-]^{(n-1)+}/(n-1)$	449.4 (449.2)	350.2 (350.2)	417.8 (417.2)	326.4 (326.1)	417.4 (417.2)	326.6 (326.1)
$[P^{n+} + 2HFBA^-]^{(n-2)+}/(n-2)$	780.2 (780.4)	537.7 (537.9)	732.9 (732.2)	505.6 (505.8)	732.1 (732.2)	506.2 (505.8)
$[P^{n+} + 3HFBA^-]^{(n-3)+}/(n-3)$		913.0 (913.3)		864.8 (865.2)		865.8 (865.2)
$[H_2P]^{4+}/4$	283.6 (283.7)		260.2 (259.6)		259.9 (259.6)	
$[H_2P^{4+} - H^+]^{3+}/3$	378.1 (377.9)		346.5 (345.8)			
$[P^{n+} + H^+ + 2HFBA^-]^{(n-1)+}/(n-1)$					488.9 (488.5)	
$[P^{n+} - H^+ + HFBA^-]^{(n-2)+}/(n-2)$	673.3 (673.4)		625.9 (625.2)			
$[P^{n+} + H^+ + 3HFBA^-]^{(n-2)+}/(n-2)$	887.0 (887.3)				840.3 (839.2)	

[a]~1 μM solution of porphyrins and metalloporphyrins in 1/1 v/v acetonitrile/H_2O [containing 0.01% v/v heptafluorobutyric acid (HFBA)] mixture, 20 V cone voltage; n = 4 or 5 corresponding to H_2P or MnP accordingly.

the purity of the sample. Data are summarized in Table 2. All MS spectra are provided in Supporting Information (Figure S4).

Lipophilicity. Both TLC retention factor, R_f (compound path/solvent path), and the partition coefficient between n-octanol and water, log P_{OW}, are equally valid parameters in assessing lipophilicity of the free ligands and their Mn complexes.[79,81] R_f was obtained on silica gel plates using acetonitrile/KNO_3(sat)/water = 8/1/1 as previously described.[81] As it is difficult to impossible to fully reproduce the R_f values from one experiment to another, we are routinely comparing all the compounds of interest in a single experiment. The log P_{OW} values of the newly synthesized compounds were determined as reported by Kos et al.[81] The log P_{BW} values (the partition between water-saturated n-butanol and n-butanol-saturated water) were determined experimentally using the following equation: log P_{BW} = log(C_{nBuOH}/C_{water}). The log P_{BW} values were converted to log P_{OW} using the equation: log P_{OW} = 1.55 × log P_{BW} − 0.54.[81,82] The log P_{OW} values for the most hydrophilic porphyrins, MnTE-2-PyP^{5+} and MnTE-3-PyP^{5+}, were determined using the following equations: log P_{OW} = 12.207 × R_f − 8.521 for *ortho* Mn(III) *N*-alkylpyridyl porphyrins (i.e., MnTE-2-PyP^{5+}), and log P_{OW} = 8.764 × R_f − 8.198 for *meta* Mn(III) *N*-alkylpyridyl porphyrins (i.e., MnTE-3-PyP^{5+}).[81,83] The R_f and log P_{OW} values are given in Table 3.

Table 3. Lipophilicity of MnPs Determined in Terms of TLC Retention Factor, R_f, and Partition Coefficient between n-Octanol and Water, log P_{OW}

Mn porphyrin	lipophilicity	
	R_f[a]	log P_{ow}[b]
MnTE-2-PyP^{5+}	0.07	−7.67[c]
MnTE-3-PyP^{5+}	0.12	−7.15[c]
MnTnHexOE-2-PyP^{5+}	0.50(0.53)	−1.67
MnTPhE-2-PyP^{5+}	0.40(0.47)	−5.90
MnTE-2-PyPhP^{5+}	0.32(0.45)	−5.51
MnTnOct-2-PyP^{5+}	0.48	−2.27

[a]Lipophilicities of porphyrin ligands of the related Mn complexes are given in parentheses. The TLC was done on silica gel plates using acetonitrile/KNO_3(sat)/water = 8/1/1 as a mobile phase. [b]Determined experimentally using n-butanol and water biphasic system and converted to log P_{OW} according to the equation log P_{OW} = 1.55 × log P_{BW} − 0.54; P_{BW} is the partition between n-butanol and water.[81,82] [c]Data obtained from R_f vs log P_{OW} relationships.[81,83]

Electrochemistry. Cyclic voltammetry measurements were performed under argon in a glass cell on CH Instruments model 600 voltammetric analyzer, as described previously.[5,84] Stock solutions of MnPs were prepared by dissolving solids in deionized water. Working solutions of ~0.2 mM MnPs were prepared in 0.05 M phosphate buffer (pH = 7.8). The supporting electrolyte in all measurements was 0.1 M NaCl. The pH values were determined on a Denver Instrument Model 250 pH-meter using a glass electrode calibrated with the standard buffers (pH 4.00, 7.00, and 10.00). The concentrations of MnPs were determined spectrophotometrically. All potentials are reported versus the normal hydrogen electrode (NHE). MnTE-2-PyP^{5+} with $E_{1/2}$ = +228 mV versus NHE was used as a reference.[16,80,81] Its voltammetry was performed before and after each series of measurements. The data are presented in Table 4.

Catalysis of $O_2^{\bullet-}$ Dismutation (Cytochrome *c* Assay). The ability of newly synthesized Mn metalloporphyrins to dismute $O_2^{\bullet-}$ was evaluated via cytochrome *c* assay. The validity of assay was proven with pulse radiolysis and stopped-flow methodology.[84−88] The cyt *c* assay is based on $O_2^{\bullet-}$ production via xanthine/xanthine oxidase reaction and metalloporphyrin ability to compete with ferricytochrome *c* in scavenging $O_2^{\bullet-}$. The experiments were conducted at room temperature (25 ± 1) °C in 0.05 M potassium phosphate buffer, pH 7.8, and 0.1 mM EDTA as previously described in detail.[84] The reduction of cytochrome *c* was followed at 550 nm. MnTE-2-PyP^{5+} was used as a standard. Data are summarized in Table 4. Kinetic traces, plots ((v_0/v_i) −1) vs [MnP]) for the calculations of IC_{50}, and the information on the calculation of $k_{cat}(O_2^{\bullet-})$ from such plots are provided in Figures S12 and S13 of Supporting Information.

Peroxynitrite Reduction with $Mn^{III}P$. Oxidation of $Mn^{III}Ps$ with peroxynitrite was carried out under pseudo-first-order conditions with peroxynitrite in excess over MnP. In all cases, peroxynitrite (dissolved in a NaOH) was mixed with MnPs dissolved in sodium phosphate buffer. The final concentrations upon mixing were the following: MnPs 0.5 μM (1 μM for MnTnHexOE-2-PyP^{5+}), 10-fold excess of peroxynitrite, and 0.05 M sodium phosphate buffer, pH 7.4, 0.1 mM DTPA. The temperature was maintained at (37.0 ± 0.1) °C, and the pH of the reaction mixtures was measured at the outlet of the stopped flow. The reaction was monitored as a change in the absorbance of the Soret band at the following: 456 nm for MnTPhE-2-PyP^{5+}, 455 nm for MnTnHexOE-2-PyP^{5+}, 467 nm for MnTE-2-PyPhP^{5+}, 454 nm for MnTE-2-PyP^{5+}, and 460 nm for MnTE-3-PyP^{5+}. The pseudo-first-order rate constants, k_{obs} (s^{-1}), were determined by fitting the stopped-flow data to a single exponential function. The second-order rate constant was determined from the slope of k_{obs} versus [$ONOO^-$] plot. All kinetic runs were performed on a stopped-flow spectrophotometer (Applied Photophysics, SX20). Data are summarized in Table 4. The raw data (kinetic traces, k_{obs} versus [$ONOO^-$] plots, and time-resolved equilibrium spectra for all new compounds are provided in Supporting Information (Figures S5−S11).

Lipid Peroxidation Assay. The lipid peroxidation was triggered spontaneously. Rat brains were homogenized on ice in 5 volumes (w/v) of cold 50 mM potassium phosphate buffer, pH 7.00. The 200 μL aliquots were diluted to a final volume of 1.0 mL with 50 mM potassium phosphate buffer and incubated 30 min at 37 °C on a shaking water bath. Under such standardized conditions the 2.2 ± 0.18 μmol/L malondialdehyde (MDA) was produced. If MDA production was not within specified limits, the homogenate was discarded. The level of MDA produced under standardized conditions was taken as 100% lipid peroxidation. In order to measure preformed MDA, as well

dx.doi.org/10.1021/ic501329p | Inorg. Chem. 2014, 53, 11467−11483

Table 4. Metal-Centered Reduction Potential, $E_{1/2}$ vs NHE of $Mn^{III}P/Mn^{II}P$ Redox Couple, Proton Dissociation Constant of First Axial Water, pK_{a1}, log $k_{cat}(O_2^{\bullet-})$ for the Catalysis of $O_2^{\bullet-}$ Dismutation, log $k_{red}(ONOO^-)$ for the $ONOO^-$ Reduction, and Initial Rates for the Catalysis of Ascorbate HA^- Oxidation with MnPs, $v_0(HA^-$ Oxidation). Relative Molecular Masses, M_r are Listed Also

compd	M_r	pK_{a1}	$E_{1/2}$, mV vs NHE[a]	log k_{cat} $(O_2^{\bullet-})$[b]	log k_{red} $(ONOO^-)$[c]	v_0 (HA^- oxidation), nM s^{-1}[d]
$MnTBAP^{3-}$	842.7	12.6[4]	−194[79]	3.16[79]	5.02[79]	2.26
$MnTE\text{-}2\text{-}PyPhP^{5+}$	1269.5	12.0[e]	−65	5.55	5.93	18.24
$MnTE\text{-}3\text{-}PyP^{5+}$	965.1	11.5[4]	54[79]	6.65[79]	6.81	229.96
$MnTE\text{-}2\text{-}PyP^{5+}$	965.1	11.0[4]	228[79]	7.76[79]	7.53[4]	312.84
$MnTPhE\text{-}2\text{-}PyP^{5+}$	1269.5	10.8[e]	259	7.66	7.14	147.21
$MnTnHexOE\text{-}2\text{-}PyP^{5+}$	1365.8	10.7[e]	313	7.92	7.61	76.33
$MnTnOct\text{-}2\text{-}PyP^{5+}$	1301.8	10.5[4]	340	7.71[79]	7.15[79]	54.29

[a] $E_{1/2}$ of $Mn^{III}P/Mn^{II}P$ redox couple is determined in 0.05 M phosphate buffer (pH 7.8, 0.1 M NaCl). [b] $k_{cat}(O_2^{\bullet-})$ is determined by cytochrome *c* assay in 0.05 M potassium phosphate buffer [pH 7.8, at (25 ± 1) °C]. [c] $k_{red}(ONOO^-)$ is determined by stopped-flow technique in 0.05 M potassium phosphate buffer [pH 7.4, at (37 ± 0.1) °C]. [d] v_0, initial rate for HA^- oxidation, was determined spectrophotometrically under aerobic conditions: 5 μM MnP, 0.15 mM sodium ascorbate, 5 mM EDTA, pH 7.4 maintained with 0.05 M Tris buffer and at (25 ± 1) °C. The mono-deprotonated HA^- is the main ascorbate species at pH 7.8. [e] pK_{a1} values were estimated on the basis of the relationship pK_{a1} vs $E_{1/2}$ of $Mn^{III}P/Mn^{II}P$ redox couple published in ref 4.

as the MDA generated during tissue handling and homogenization, butylated hydroxytoluene (BHT) was added before incubation to a final concentration of 60 mM. The MDA content of samples containing BHT did not exceed 0.0254 ± 0.0897 μmol MDA per L homogenate. After 60 min of incubation at 37 °C, BHT (60 mM) was added to all samples, and MDA was initially assessed by colorimetric thiobarbituric acid (TBA) assay.[89] The TBA assay lacks specificity. Thus, all the results were re-evaluated by HPLC analysis as previously described.[90]

Catalysis of Ascorbate Oxidation with MnPs. Initial rates of MnP-catalyzed ascorbate, HA^-, oxidation to ascorbyl radical, $HA^{\bullet}$ (which readily deprotonates to $A^{\bullet}$), were determined with 5 μM metalloporphyrin, 5 mM EDTA, and 0.15 mM sodium ascorbate under aerobic conditions at (25 ± 1)°C and at pH 7.4 maintained with 0.05 M Tris buffer. The buffer was initially treated with Chelex-100 ion-exchange resin (200−400 mesh sodium form, Bio-Rad Life Science) to remove the adventitious metals present in the solution. Ascorbate oxidation was followed at 265 nm on UV−vis spectrophotometer (Shimadzu UV-2550). The molar absorptivity of ascorbate was re-evaluated to be ε_{265} = 14 000 M^{-1} cm^{-1}. The initial rates, v_0's (HA^- oxidation) (nMs^{-1}), which were calculated on the basis of the linear kinetic traces obtained for the first 100 s, are summarized in Table 4. The background rate for noncatalyzed ascorbate oxidation was subtracted from the catalyzed reaction rates.[77]

Superoxide-Specific Biological Models. Aerobic Growth of *S. cerevisiae*. *S. cerevisiae* strains with mutations in the cytoplasmic CuZnSOD gene (sod1Δ) exhibit amino-acid auxotrophies for lysine and methionine. Only those compounds which are capable of catalyzing the dismutation of superoxide at a rate higher than $O_2^{\bullet-}$ self-dismutation substitute for the missing SOD enzyme, thus restoring the aerobic growth of a mutant in a medium lacking lysine or methionine.[67] Such growth impairment makes the SOD-deficient yeast a good system for testing the therapeutic potential of an SOD mimic. The wild type *S. cerevisiae* strain used in this study was EG103, while its corresponding sod1Δ mutant was EG118.[91,92] Stock and test cultures were grown as previously described.[67] Tests were performed in 96-well plates in triplicates. Aqueous solutions of MnPs were filter-sterilized (0.22-μm filter, Whatman, Middlesex, U.K.) and added to wells containing 200 μL aliquots of yeast culture in SD medium supplemented with all amino acids except methionine. Cultures in 96-well plates were grown aerobically at 30 °C and 220 rpm on a thermostatic shaker. Since yeast cells tend to clump irrespective of the vigorous shaking, wells were mechanically stirred at regular time intervals using a specifically designed 96-pin sterilized stirrer. In control samples the volume of MnP solution was compensated with sterile distilled water. Growth was followed turbidimetrically at 600 nm using ELISA reader.

RESULTS AND DISCUSSION

The series of MnPs, $MnTnOct\text{-}2\text{-}PyP^{5+}$, $MnTPhE\text{-}2\text{-}PyP^{5+}$, $MnTnHexOE\text{-}2\text{-}PyP^{5+}$, and $MnTE\text{-}2\text{-}PyPhP^{5+}$, was synthesized and characterized (Figure 2). With the same porphyrin core, all *meso* substituents have 8 carbon atoms differently organized in either linear or cyclic conformations resulting in compounds of vastly different properties.

Two porphyrins, $MnTnOct\text{-}2\text{-}PyP^{5+}$ and $MnTnHexOE\text{-}2\text{-}PyP^{5+}$, bear linear 8 atom-long and 9 atom-long pyridyl substituents, respectively (Figure 2). The latter has one oxygen atom buried so deeply in each of 4 alkylpyridyl chains that the surrounding medium does not sense them. In turn, the lipophilicity of $MnTnHexOE\text{-}2\text{-}PyP^{5+}$ is higher than of $MnTnOct\text{-}2\text{-}PyP^{5+}$. On the basis of a large amount of lipophilicity measurements reported,[16,80,81,93] we can safely assume that lipophilicity of $MnTnHexOE\text{-}2\text{-}PyP^{5+}$ will be similar to that of $MnTnNon\text{-}2\text{-}PyP^{5+}$ (Mn(III) *meso*-tetrakis(*N*-n-nonylpyridinium-2-yl)porphyrin). Both compounds have equal 9-atom long pyridyl substituents, but the latter does not contain oxygen atoms.

Two other porphyrins, $MnTPhE\text{-}2\text{-}PyP^{5+}$ and $MnTE\text{-}2\text{-}PyPhP^{5+}$, bear two cyclic aromatic rings, one phenyl and one pyridyl. The rings are differently organized: in $MnTPhE\text{-}2\text{-}PyP^{5+}$, the pyridyl ring precedes phenyl, and in $MnTE\text{-}2\text{-}PyPhP^{5+}$ the pyridyl ring follows phenyl ring (Figure 2). In the first case the positively charged quaternary nitrogen atoms are close to the metal site and affect favorably the $E_{1/2}$. In the second case they are far away, separated from the porphyrin core by the phenyl ring and in turn have minimal impact on $E_{1/2}$. Besides the effect on $E_{1/2}$, such distribution of charges affects differentially the shape of the molecule, and in turn the solvation/lipophilicity of these MnPs and their interactions with biotargets.

Compounds were characterized in terms of the following: (i) elemental analysis; (ii) NMR spectroscopy; (iii) UV−vis spectral properties (Table 1); (iv) electrospray mass spectrometry, ESI-MS (Table 2); (v) lipophilicity in terms of P_{OW} and R_f (Table 3); (vi) electrochemistry (metal-centered reduction potential $E_{1/2}$ of $Mn^{III}P/Mn^{II}P$ redox couple) (Table 4); (vii) ability to catalyze $O_2^{\bullet-}$ dismutation, $k_{cat}(O_2^{\bullet-})$ (Table 4); (viii) ability to reduce $ONOO^-$, $k_{red}(ONOO^-)$ (Table 4); and (ix) ability to catalyze ascorbate, HA^- oxidation, described by initial rate, $v_0(HA^-)$ (Table 4, Figure 7).

dx.doi.org/10.1021/ic501329p | Inorg. Chem. 2014, 53, 11467−11483

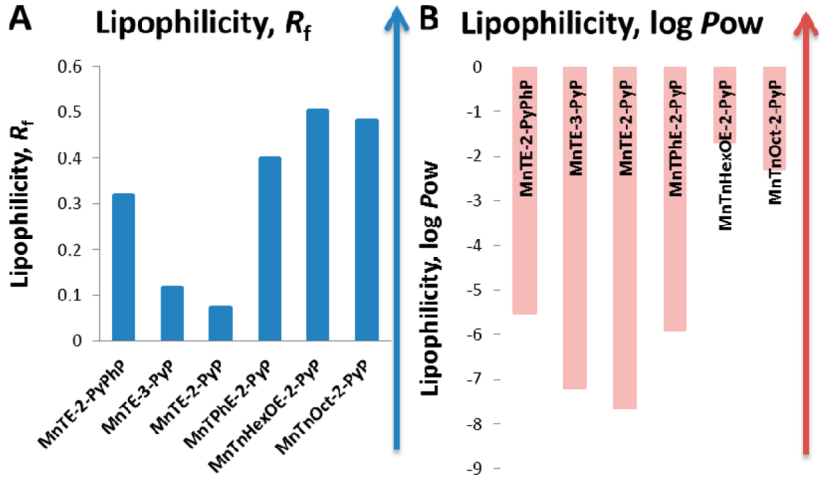

Figure 5. Lipophilicities of Mn(III) porphyrins expressed in terms of chromatographic retention factor, R_f (A), and partition coefficient between n-octanol and water, log P_{OW} (B). The R_f values are linearly related to log P_{OW} values.[81,93] The small differences in R_f values translate into large differences in log P_{OW} values.[81,93]

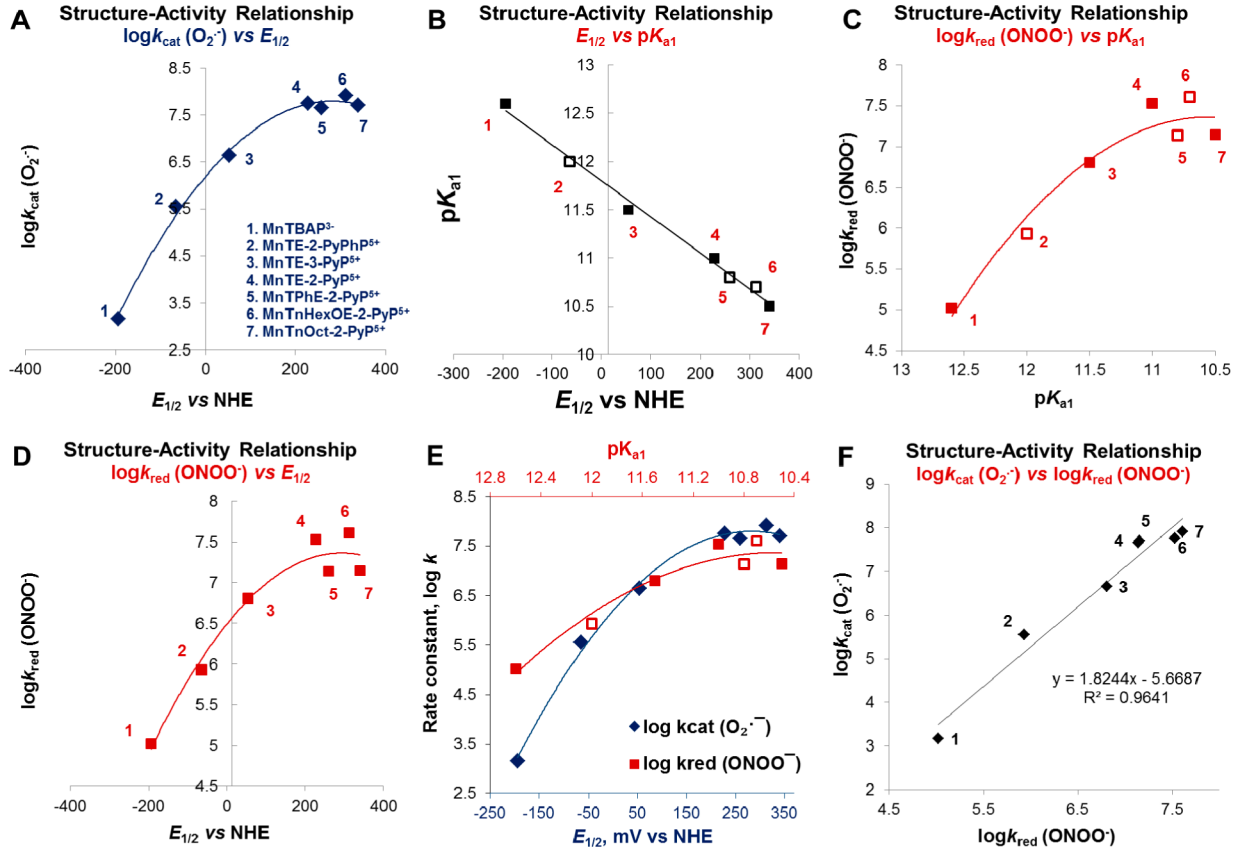

Figure 6. Structure−activity relationships between the kinetic parameters, log k_{cat} ($O_2^{\bullet-}$) and log k_{red} ($ONOO^-$), and thermodynamic parameters, $E_{1/2}$ for $Mn^{III}P/Mn^{II}P$ redox couple (mV vs NHE), and proton dissociation constant of first axial water, pK_{a1}. (A) log k_{cat}($O_2^{\bullet-}$) vs $E_{1/2}$ for $Mn^{III}P/Mn^{II}P$ redox couple; (B) pK_{a1} vs $E_{1/2}$ for $Mn^{III}P/Mn^{II}P$ redox couple; (C) log k_{red} ($ONOO^-$) vs pK_{a1}; (D) log k_{red} ($ONOO^-$) vs $E_{1/2}$ for $Mn^{III}P/Mn^{II}P$ redox couple; (E) log k_{red} ($ONOO^-$) vs pK_{a1} and log k_{cat}($O_2^{\bullet-}$) vs $E_{1/2}$ for $Mn^{III}P/Mn^{II}P$ redox couple; (F) log k_{cat}($O_2^{\bullet-}$) vs log k_{red} ($ONOO^-$) . Numerical values and experimental conditions for k_{cat} ($O_2^{\bullet-}$), k_{red} ($ONOO^-$), pK_{a1}, and $E_{1/2}$ (mV vs NHE) are given in Table 4; empty squares in parts B, C, and E are estimated values: (1) MnTBAP^{3-}, (2) MnTE-2-PyPhP^{5+}, (3) MnTE-3-PyP^{5+}, (4) MnTE-2-PyP^{5+}, (5) MnTPhE-2-PyP^{5+}, (6), MnTnHexOE-2-PyP^{5+}, and (7) MnTnOct-2-PyP^{5+}. The kinetics of $Mn^{III}P$ oxidation to O=$Mn^{IV}P$, involved in reduction of $ONOO^-$ as well as reduction of lipid reactive species (see Figure 8), relates to the thermodynamics of $Mn^{III}P/Mn^{II}P$ redox couple. For explanation, see text; in brief, the electron transfer from Mn to $ONOO^-$ is preceded with $ONOO^-$ ligand binding which is dependent upon the electron-deficiency of Mn site. The latter is described by proton dissociation equilibrium of first axial water, pK_{a1}, which parallels $E_{1/2}$ of $Mn^{III}P/Mn^{II}P$ redox couple and is shown in part B.[4,76] There appears to be no difference between the $E_{1/2}$ values for O=$Mn^{IV}P/Mn^{III}P$ for various structurally diverse metalloporphyrins (Supporting Information Table S1).

dx.doi.org/10.1021/ic501329p | *Inorg. Chem.* 2014, 53, 11467−11483

Lipophilicity of MnPs. The linear relationship between the chromatographic retention factor, R_f, and log P_{OW} has been established for water-soluble cationic Mn *N*-alkylpyridylporphyrins.[77,92] It guided us not only in the design and development of lead drug candidates but also in the safe prediction of the partition coefficients of those compounds which are highly hydrophilic and for which log P_{OW} could not be assessed, such as MnTE-2-PyP^{5+} and MnTE-3-PyP^{5+}.[81,94] The log P_{OW} and R_f values of the series of ligands and related MnPs are listed in Table 3 and Figure 5 and are related to other properties of MnPs in Figure 6. While water-soluble MnPs do not distribute readily into n-octanol (as illustrated by highly negative log P_{OW} value), multiple positive charge is a driving force for their distribution into brain and mitochondria.[83] In mitochondria they mimic mitochondrial matrix MnSOD.[83,95−97]

The different reorganization of 8 carbon atoms in *meso* substituents resulted in the following observations depicted in Figure 5: (1) lipophilicity of the molecule dropped noticeably by >3.5 log units when 8-carbon atom alkyl chains rearrange into aromatic phenyl or pyridyl substituents; (2) significant increase in lipophilicity was observed when an oxygen atom was introduced into n-octyl chains to form n-hexoxyethyl chains [log P_{OW} (MnTnOct-2-PyP^{5+}) < log P_{OW} (MnTnHexOE-2-PyP^{5+})]. We have previously reported that the introduction of one methoxy group at the periphery of each of four hexyl chains reduced significantly the lipophilicity of MnTMOHex-3-PyP^{5+} relative to MnTnHex-3-PyP^{5+}.[80] Such a drop was considerably minimized when the oxygen atoms were buried deeper into the alkyl chains of MnTnBuOE-2-PyP^{5+}.[16] Consequently, this porphyrin has only slightly lower lipophilicity relative to MnTnHex-2-PyP^{5+} [log P_{OW} (MnTnBuOE-2-PyP^{5+}) = −4.10 versus log P_{OW} (MnTnHex-2-PyP^{5+}) = −3.86]. The oxygen atoms in MnTnHexOE-2-PyP^{5+} are buried even deeper within the lipophilic n-octyl chains. In turn, the solvation is largely suppressed. We can predict that the chains of a n-hexoxyethyl analog would behave similarly to linear 9-carbon atom substituents in MnTnNon-2-PyP^{5+}; the latter is estimated to have partition coefficient log P_{OW} = −1.18 based on reported data for a series of Mn(III) *N*-alkylpyridylporphyrins.[81,94]

With phenyl rings at the periphery, such as in MnTPhE-2-PyP^{5+}, the compound is more lipophilic than MnTE-2-PyPhP^{5+} where the pyridyl cationic charges are exposed at the periphery. As expected, both compounds are much more lipophilic than either MnTE-2-PyP^{5+} or MnTE-3-PyP^{5+}.

Structure−Activity Relationships among $E_{1/2}$, pK_{a1}, $k_{cat}(O_2^{\bullet-})$, and k_{red}(ONOO$^-$). Cationic Mn(III) porphyrins are among the most potent SOD mimics. They have been tested in numerous oxidative stress related models and have shown remarkable therapeutic potential which is attributed to their ability to interact not only with $O_2^{\bullet-}$, but also with numerous other reactive species, such as ONOO$^-$, $CO_3^{\bullet-}$, H_2O_2, ClO$^-$, ascorbate, lipid reactive species, and thiols, RS$^-$.[2] Data, thus far obtained, provide evidence that the ability of MnP to efficiently eliminate $O_2^{\bullet-}$ closely parallels its therapeutic efficacy.[2] As already noted in the Introduction, this is due to the appropriate electron-deficiency of Mn site which favors reactions with nucleophiles, not only $O_2^{\bullet-}$ but other species, some of which are listed above. SOD enzymes have the same thermodynamic property of metal site as MnPs, but steric hindrance imposed by large protein structure provides specificity toward $O_2^{\bullet-}$. Thus, their reactivity toward other species is a few orders of magnitude lower than that of SOD mimics.

In order to mimic the kinetics and thermodynamics of the enzymatic catalysis of $O_2^{\bullet-}$ dismutation (eqs 1 and 2), the metal-centered reduction potential should be around the midpoint (∼+300 mV vs NHE) between the potential for the oxidation (−180 mV vs NHE) and reduction of $O_2^{\bullet-}$ (+890 mV vs NHE).[98−100] Such $E_{1/2}$ is controlled by *ortho*-positioned positively charged quaternary pyridyl nitrogens (pyridyls directly linked to porphyrin macrocycle at *meso* positions) which provide equal thermodynamics for both steps of the dismutation process and ensure favorable electrostatics for the approach of negatively charged $O_2^{\bullet-}$ molecule to the metal site (eqs 1 and 2). The porphyrin solvation impacts the $E_{1/2}$ also.[13] A perfect SOD mimic should oxidize (k_{ox}, eq 1) and reduce (k_{red}, eq 2) $O_2^{\bullet-}$ with nearly identical rate constants which for SOD enzyme are $k_{ox} \approx k_{red} \sim 10^9$ M^{-1} s^{-1}. We have reported that this is indeed true for MnTE-2-PyP^{5+} whose log $k_{cat}(O_2^{\bullet-})$ = 7.76 and $E_{1/2}$ = +228 mV versus NHE.[101] It is presumably valid for cationic *ortho* Mn(III) pyridylporphyrins (MnTnOct-2-PyP^{5+}, MnTnHexOE-2-PyP^{5+}, and MnTPhE-2-PyP^{5+}) also, as all of them have $E_{1/2}$ values of ∼+300 mV versus NHE and exhibit a high ability to catalyze $O_2^{\bullet-}$ dismutation, log $k_{cat}(O_2^{\bullet-}) \sim 7.8$ (Table 4). In addition to eq 1, Mn^{III}P could be reduced to Mn^{II}P with ascorbate shown by eq 1b, and reoxidized with $O_2^{\bullet-}$ to Mn^{III}P acting as superoxide reductase like rubredoxin oxidoreductase,[102] a likely scenario *in vivo* due to the abundance of ascorbate.

$$Mn^{III}P^{5+} + O_2^{\bullet-} \Leftrightarrow Mn^{II}P^{4+} + O_2 \quad k_{ox}(O_2^{\bullet-}) \tag{1}$$

$$Mn^{III}P^{5+} + HA^- \Leftrightarrow Mn^{II}P^{4+} + HA^{\bullet}(HA^{\bullet} \rightarrow A^{\bullet-} + H^+) \quad k_{ox}(HA^-) \tag{1b}$$

$$Mn^{II}P^{4+} + 2H^+ + O_2^{\bullet-} \Leftrightarrow Mn^{III}P^{5+} + H_2O_2 \quad k_{red}(O_2^{\bullet-}) \tag{2}$$

Mn^{III}P reduces ONOO$^-$ via one-electron reaction giving rise to toxic $^{\bullet}NO_2$ (eq 3).[5] *In vivo*, the reduction of ONOO$^-$ by MnP is likely coupled to cellular reductants such as ascorbate.[5] In a first step Mn^{III}P gets reduced with ascorbate to Mn^{II}P (eq 1b). In a subsequent step Mn^{II}P gets oxidized two-electronically to O=Mn^{IV}P while benign nitrite, NO_2^-, is formed. The rate constant for reaction 4 has been estimated for MnTE-2-PyP^{5+}, and is equal or higher than for the reaction given by eq 3.[6] The O=Mn^{IV}P is a highly oxidizing species. Its damage to biological targets is largely suppressed at the expense of cellular reductants as they readily reduce it to Mn^{III}P.[5]

$$Mn^{III}P^{5+} + ONOO^- \Leftrightarrow O{=}Mn^{IV}P^{4+} + {}^{\bullet}NO_2 \quad k_{red1}(ONOO^-) \tag{3}$$

$$Mn^{II}P^{4+} + ONOO^- \Leftrightarrow O{=}Mn^{IV}P^{4+} + NO_2^- \quad k_{red2}(ONOO^-) \tag{4}$$

The $E_{1/2}$ of Mn^{III}P/Mn^{II}P redox couple for the series of compounds studied varies from −194 to +340 mV versus NHE. Strong correlations have been found between $E_{1/2}$ and $k_{cat}(O_2^{\bullet-})$ (eqs 1 and 2; Figure 6A). We observed earlier with Mn(III) *N*-alkylpyridylporphyrins,[4] and here with new series of porphyrins, that k_{red}(ONOO$^-$) correlates with $E_{1/2}$ for Mn^{III}P/Mn^{II}P even though the reaction of MnP with

dx.doi.org/10.1021/ic501329p | Inorg. Chem. 2014, 53, 11467−11483

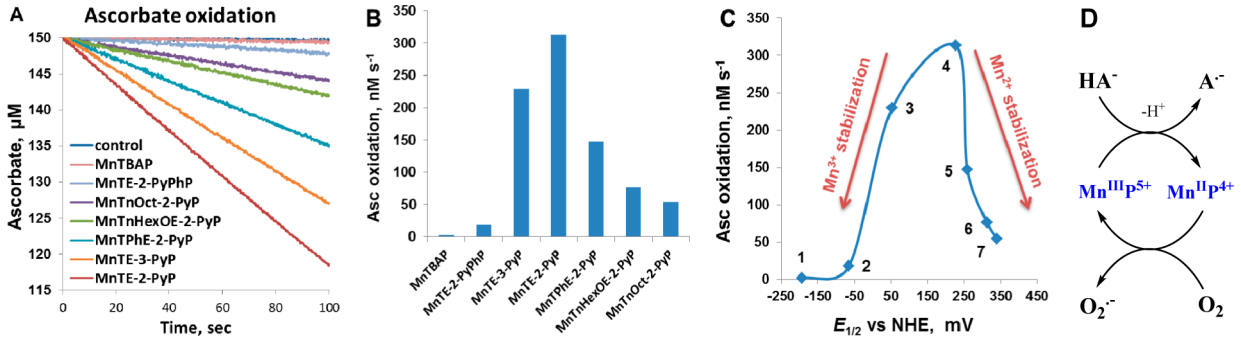

Figure 7. MnP-catalyzed ascorbate oxidation. (A) Kinetic traces for different MnPs. (B) Initial rates of ascorbate oxidation/consumption expressed in nM s^{-1}. (C) Regions where $E_{1/2}$ Mn is stabilized in +2 and +3 oxidation states; MnTE-2-PyP^{5+} is the most optimized MnP in terms of H_2O_2 production. It has equally stabilized +2 and +3 oxidation states.[101] It gets readily reduced with ascorbate but also reoxidized back to $Mn^{III}P$ with either $O_2^{\bullet-}$ or O_2, whichever is *in vivo* in excess. Those MnPs with negative potentials do not favor reduction, while those with too positive potential do not favor reoxidation of $Mn^{II}P$. (D) Redox cycling of MnP with ascorbate, which involves the reoxidation of $Mn^{II}P$ with O_2 (preferred over $O_2^{\bullet-}$ due to its higher *in vivo* levels) to close the catalytic cycle. The conditions are 5 μM MnP, 0.15 mM sodium ascorbate at pH 7.4 maintained with 0.05 M Tris buffer with 5 mM EDTA, (25 ± 1) °C. The numerical assignments in part C are identical to those described in the Figure 6 caption.

peroxynitrite, studied in this work, involves the $O{=}Mn^{IV}P/Mn^{III}P$ redox couple. This can be accounted for by a two-step process: (i) binding of $ONOO^-$ to the Mn site, and (ii) subsequent reduction of $ONOO^-$ yielding $O{=}Mn^{IV}P$ species. The first step is dependent upon the Mn site electron-deficiency, a property well-described by the $E_{1/2}$ of $Mn^{III}P/Mn^{II}P$ couple. This $E_{1/2}$ has previously been reported to linearly correlate (i) with metal-free porphyrin protonation equilibria of its inner pyrrolic nitrogens,[76] and (ii) with the protonation equilibria of axial waters of MnPs, depicted herein with the proton dissociation constant of first axial water, pK_{a1} (eq 5 and Figure 6B).[4]

$$(H_2O)_2Mn^{III}P^{5+} \Leftrightarrow (H_2O)(OH)Mn^{III}P^{4+} + H^+ \quad pK_{a1} \tag{5}$$

Therefore, the MnPs of more positive $E_{1/2}$ for $Mn^{III}P/Mn^{II}P$ redox couple and lower pK_{a1} values (Figure 6B) are more electron-deficient and favor binding of an electron-rich ligand ($ONOO^-$ in this case) which in turn gives rise to higher $k_{red}(ONOO^-)$ (Figure 6C).[2] Such data explain why the log $k_{red}(ONOO^-)$ correlates as well with $E_{1/2}$ for $Mn^{III}P/Mn^{II}P$ (Figure 6D) as does log $k_{cat}(O_2^{\bullet-})$ (Figure 6A). It thus explains why there is a linear relationship between log $k_{red}(ONOO^-)$ and $k_{cat}(O_2^{\bullet-})$ (Figure 6F). The second step of the reaction of $Mn^{III}P$ with $ONOO^-$ is related to the $E_{1/2}$ values for the $O{=}Mn^{IV}P/Mn^{III}P$ couple. These, as well as those for $(O)_2Mn^{V}P/Mn^{III}P$ redox couples, are essentially identical for different Mn and Fe porphyrins.[5,103−110] All relevant reduction potentials are listed in Supporting Information (Table S1).[4,5,76,111,112] For example, the $E_{1/2}$ values for $Mn^{III}P/Mn^{II}P$ redox couple of MnTE-2-PyP^{5+}, MnTE-3-PyP^{5+}, and MnTnBu-2-PyP^{5+} differ by up to 176 mV, while $E_{1/2}$ for $O{=}Mn^{IV}P/Mn^{III}P$ redox couple values are +509, +529, and +509 mV versus SHE at pH 11, respectively (Supporting Information Table S1).[112] Further, $E_{1/2}$ values for $O{=}Mn^{IV}P/Mn^{III}P$ of MnTM-2-PyP^{5+}, MnTM-3-PyP^{5+}, and MnTM-4-PyP^{5+} are +540, +526, and +532 mV versus NHE at pH 11, while $E_{1/2}$ values for their $Mn^{III}P/Mn^{II}P$ redox couples differ by up to 168 mV (Table 4 and Supporting Information Table S1).[5] Finally, $E_{1/2}$ values for the $(O)_2Mn^{V}P/Mn^{III}P$ redox couple for MnTM-4-PyP^{5+}, MnTM-2-PyP^{5+}, and MnTDM-2-ImP^{5+} (Mn(III) *meso*-tetrakis(*N*,*N*′-dimethylimidazolium-2-yl)porphyrin) at pH 11 are all around +800 mV versus NHE, while their $E_{1/2}$ values for the $Mn^{III}P/Mn^{II}P$ redox couple differ by up to 260 mV (Supporting Information Table S1).[111] Thus, the only factor different among these MnPs with respect to their oxidation to oxo-Mn species is the binding of highly oxidizing species (such as $ONOO^-$, H_2O_2, and lipid reactive species) to Mn, a rate limiting step dependent upon the electron deficiency/richness of Mn site and thus best characterized with proton dissociation constants of either porphyrin pyrrolic nitrogens, or axial waters,[4,76] or the $E_{1/2}$ value of the $Mn^{III}P/Mn^{II}P$ redox couple. Of note, as already indicated, the oxidation of MnPs with $ONOO^-$ *in vivo* may involve the $O{=}Mn^{IV}P/Mn^{II}P$ redox couple (eq 4), as $Mn^{III}Ps$ would likely be readily reduced to $Mn^{II}Ps$ by cellular reductants. The $E_{1/2}$ of the $O{=}Mn^{IV}P/Mn^{II}P$ redox couple is controlled in part by the $Mn^{III}P/Mn^{II}P$ redox couple and thus differs among MnPs, for MnTE-2-PyP^{5+}, MnTE-3-PyP^{5+}, and MnTnBuOE-2-PyP^{5+}. The $E_{1/2}$ ($O{=}Mn^{IV}P/Mn^{II}P$) values were calculated to be +317, +253, and +343 mV versus SHE,[112] resulting in a higher driving force and therefore thermodynamically favoring the two-electron reduction of $ONOO^-$.[112]

An interesting phenomenon has been observed when two plots [log $k_{cat}(O_2^{\bullet-})$ vs $E_{1/2}$ and log $k_{red}(ONOO^-)$ vs pK_{a1}] are overlapped (Figure 6E). The differences observed between the highest and the lowest rate constants for $O_2^{\bullet-}$ dismutation and $ONOO^-$ reduction at identical $E_{1/2}$ values are 4.55 [$\Delta k_{cat}(O_2^{\bullet-})$] and 2.13 [$\Delta k_{red}(ONOO^-)$]. The diagram supports the fact that the reported beneficial effects of MnTBAP[3−18−42] could be rather attributed to its peroxynitrite reducing ability, and not superoxide scavenging.

The therapeutic effects observed with cationic *ortho* Mn(III) *N*-substituted pyridylporphyrins cannot be safely assigned to a specific reactive species. Implementing multiple approaches, including pharmacological and genetic, along with direct measurements of MnP subcellular localization may allow us to safely identify the location of MnP within tissue and cell/cellular fragments and the nature of reactive species involved in its mode of action.

MnP-Catalyzed Ascorbate Oxidation. Understanding the reactivity of MnPs toward ascorbate is biologically relevant due to the: (i) high intracellular ascorbate concentrations; (ii) high ability of MnPs to oxidize ascorbate; (iii) coupling of ascorbate with $O_2^{\bullet-}$ and $ONOO^-$; reduction of $Mn^{III}P$ to $Mn^{II}P$ with ascorbate *in vivo* is likely a first step in its redox cycling with $O_2^{\bullet-}$ and $ONOO^-$ - in such scenario MnP acts as

dx.doi.org/10.1021/ic501329p | *Inorg. Chem.* 2014, 53, 11467−11483

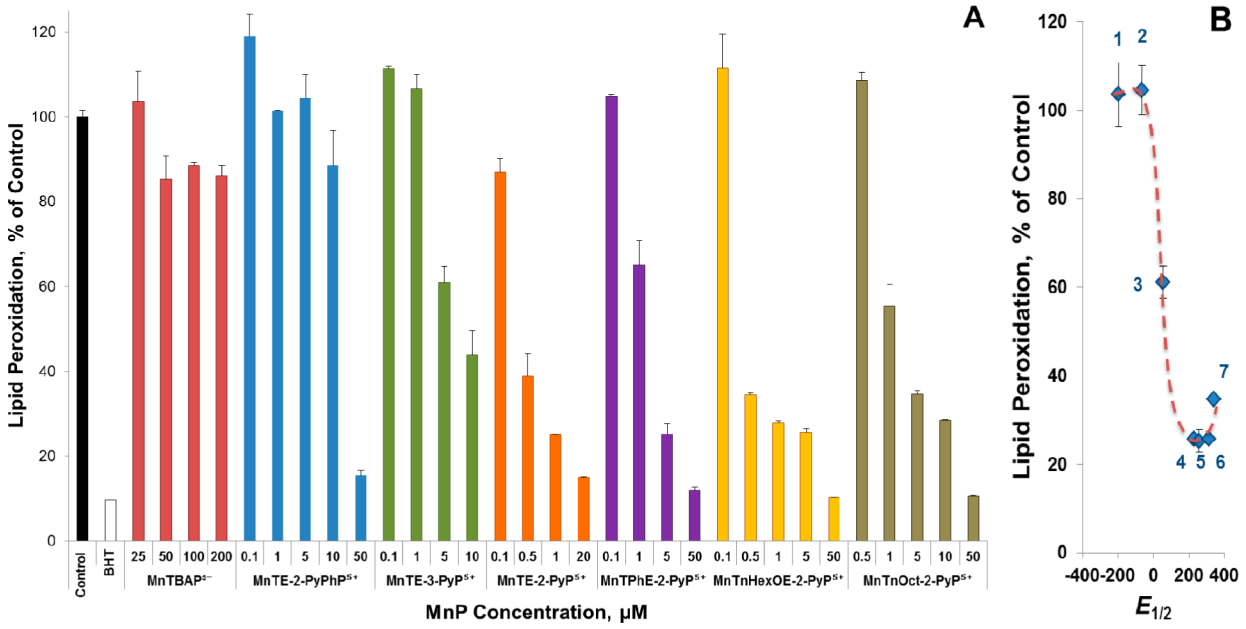

Figure 8. Attenuation of lipid peroxidation by various MnPs as a function of their of metal-centered reduction potentials. (A) The ability of MnPs to prevent lipid peroxidation of rat brain homogenates in terms of malondialdehyde, MDA, expressed as % of control (taken as 100% of lipid peroxidation) measured by HPLC method. Butylated hydroxytoluene (BHT) was used as positive control which prevented ∼90% of lipid peroxidation. The $E_{1/2}$ of $Mn^{III}P/Mn^{II}P$ governs the ability of MnPs to attenuate lipid peroxidation. The possible reasons why the oxidation of $Mn^{III}P$ with lipid reactive species relates to the $E_{1/2}$ of $Mn^{III}P/Mn^{II}P$ have been discussed in Figure 6 and in text in the Structure−Activity Relationships section. The bulkiness of the molecule, i.e., the steric hindrance toward lipid reactive species plays a minimal role. The impact of $E_{1/2}$ was better visualized in plot B where the percent of lipid peroxidation was plotted vs $E_{1/2}$ at 5 μM MnP. At that concentration, no inhibition of lipid peroxidation was observed with $MnTBAP^{3-}$ (1) and MnTE-2-$PyPhP^{5+}$ (2). As $E_{1/2}$ increases from $MnTBAP^{3-}$ and MnTE-2-$PyPhP^{5+}$ to MnTE-3-PyP^{5+}, the inhibition of lipid peroxidation increases (3) and reaches maximum at ∼+300 mV vs NHE with MnTE-2-PyP^{5+} (4), MnTPhE-2-PyP^{5+} (5), and MnTnHexOE-2-PyP^{5+} (6). The somewhat lower inhibition with MnTnOct-2-PyP^{5+} (7) is likely due to the steric hindrance imposed by long *N*-pyridyl substituents toward the approach of lipid reactive species.

$O_2^{\bullet-}$ reductase rather than superoxide dismutase;[113] and (iv) therapeutic potential of MnP/ascorbate as a ROS generator for tumor therapy.

We have herein demonstrated that the ability of MnPs to catalyze ascorbate oxidation (eq 1b), described as initial rate, $v_0(HA^-)$, depends upon the electron deficiency of the metal center, $E_{1/2}$. The bell-shape curve was established for MnPs in the range $E_{1/2}$ −194 to +340 mV versus NHE (Figure 7). The highest rate of ascorbate oxidation was reached for MnTE-2-PyP^{5+} at $E_{1/2}$ of +228 mV versus NHE, and dropped afterward. The k_{cat} $(O_2^{\bullet-})$ and k_{red} $(ONOO^-)$, though, reached a plateau at MnTE-2-PyP^{5+} but did not drop afterward (Figure 6A,D). The ratio of the stabilities of Mn +2 and +3 oxidation states has larger impact on the catalysis of ascorbate oxidation than it has on $O_2^{\bullet-}$ dismutation, where the interplay of solvation and lipophilicity of alkyl chains results in similarly high k_{cat} $(O_2^{\bullet-})$ of MnTnOct-2-PyP^{5+} and MnTE-2-PyP^{5+} (Figure 6A).[13]

We have shown that $k_{red}(O_2^{\bullet-}) = k_{ox}(O_2^{\bullet-})$ for MnTE-2-PyP^{5+} with $E_{1/2}$ = +228 mV vs NHE.[101] Thus, both +3 and +2 oxidation states are equally stabilized. With MnTnOct-2-PyP^{5+}, at +340 mV versus NHE, the Mn +2 oxidation state is more stabilized and disfavors reoxidation with either O_2 or $O_2^{\bullet-}$ (whichever species predominates *in vivo* in MnP neighborhood), suppressing in turn the cycling of MnP with ascorbate. In addition to ascorbate, glutathione and cysteine (and likely protein thiols based on their exposure) may reduce MnP also. The magnitude of the reoxidation of $Mn^{II}P$, resulting eventually in a peroxide production, may distinguish which compound would produce higher levels of H_2O_2 and be more efficient in employing it subsequently in oxidation of biological targets. The relevance of the differential impact of MnP/peroxide on cancer versus normal cell is discussed in the next paragraph.

Differential Impact of MnP/Peroxide on Cancer versus Normal Cell. The interaction of MnP with peroxide produced in its cycling with ascorbate (or when combined with radiation[114] or other chemotherapies such as dexamethasone)[10,11,114,115] will eventually cause cancer cell death, while either sparing or protecting normal cell. While little is still known on the differential biology of cancer versus normal cells, the prevailing opinion is that this is largely based on the differential redox environments of those cells; in turn, the differential impact of MnP/peroxide is dependent upon such differences also. It has been established that cancer relative to normal cell is under increased oxidative stress. While cancer cell often up-regulates MnSOD in efforts to control oxidative stress, this seems frequently not to be accompanied by up-regulation of appropriate levels of peroxide removing enzymes.[116−120] Thus, an increase in circulating MnSOD frequently results in increased peroxide levels and is positively correlated with tumor reoccurrence.[30,83] Moreover, down-regulation of a number of peroxide removing enzymes, such as thioredoxin reductase, peroxyredoxin, catalase, and glutathione peroxide, was reported;[116−120] in turn, the peroxide levels get increased as tumor progresses. Malignant properties were reportedly reversed by up-regulation of catalase.[121] Under such conditions of high oxidative stress, any addition of a redox-active compound such as MnP, that further enhances the levels of RS via cycling with cellular reductants such as ascorbate (added exogenously), will further increase the levels of superoxide/peroxide and will enhance cancer cell death, the observation we

dx.doi.org/10.1021/ic501329p | *Inorg. Chem.* 2014, 53, 11467−11483

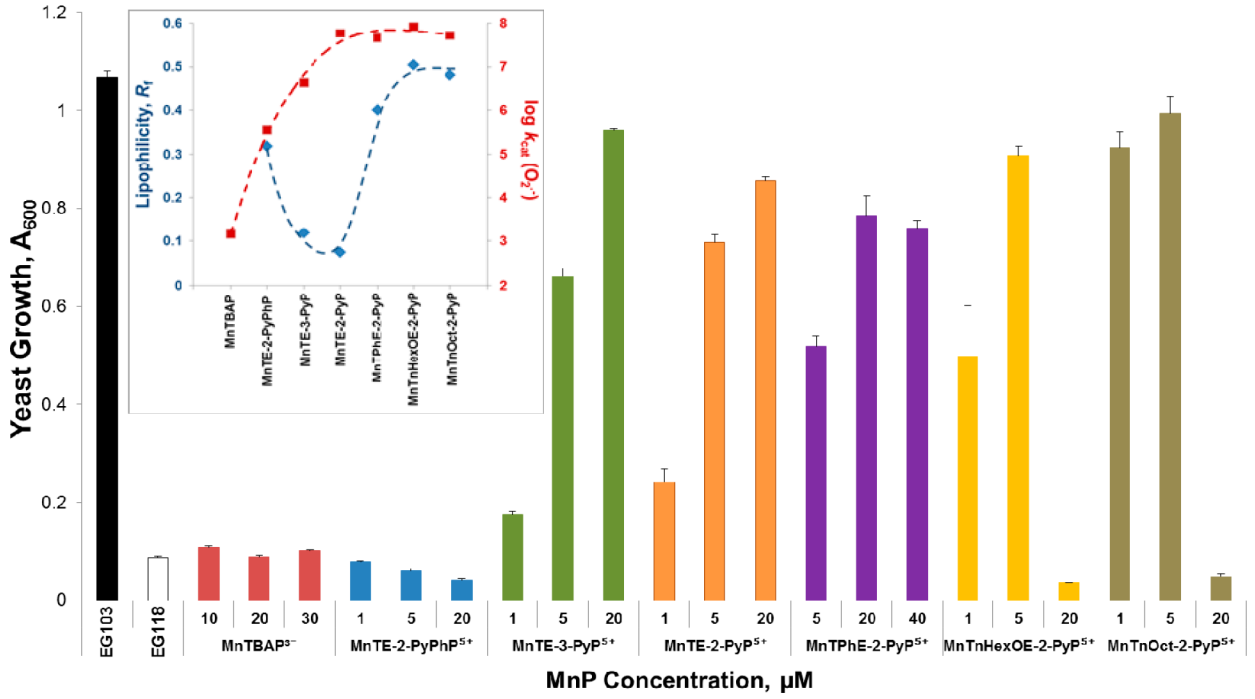

Figure 9. Aerobic growth of the wild type SOD-proficient (EG 103) and SOD-deficient (EG118) *S. cerevisiae* in the presence and absence of MnPs. Yeast grew in a restricted medium where the impact of MnPs is enhanced. All samples were run in triplicate. Growth was followed turbidimetrically by measuring the absorbance at 600 nm using ELISA reader. Inset: The lipophilicity, R_β and the SOD-like activity, described by log $k_{cat}(O_2^{\bullet-})$, are plotted to demonstrate their impact on the growth of SOD-deficient yeast. The plots show that compounds of high lipophilicity (bioavailability) and high log $k_{cat}(O_2^{\bullet-})$ are the most efficacious in protecting SOD-deficient yeast and in turn bear the highest therapeutic potential.

have frequently demonstrated.[2,77,78] Such enhancement of oxidative stress via radiation or chemotherapy has been regularly used as therapeutic modality. Thus, the enhancement of the anticancer effect in a lymphoma cellular study by the joint action of MnP and dexamethasone has been reported.[11] The cancer cell killing by MnP in a lymphoma model occurred via MnP/peroxide-driven oxidation of thiols of antiapoptotic transcription factor NF-κB with subsequent suppression of its transcription.[10,11,55,115] The inactivation of mitochondrial complexes I and III, and the impact on the glycolysis by MnP/dexamethasone, has been implicated in cancer cell death also.[10]

In a normal cell, though, the dismutation of $O_2^{\bullet-}$ catalyzed by MnP and MnP cycling with ascorbate, both giving rise to peroxide, has no significant toxic impact as peroxide is readily removed by abundant peroxide-removing enzymes maintaining physiological redox balance. If anything, and in diseased cell, the MnP may suppress excessive inflammation which would have otherwise lead to death of a normal cell. This could occur via suppression of NF-κB transcription by oxidation of its thiols, yet to a limited extent as levels of peroxide are much lower than those in a cancer cell. We have indeed frequently reported on the differential effects of MnP on normal versus cancer cells.[17,114,122,123] Please see for further discussion Miriyala et al.[83]and Batinic-Haberle et al.[2]

The type of cell, cancer or normal, will control the suitability of particular MnP as a therapeutic of choice: MnTE-2-PyP^{5+} and MnTE-3-PyP^{5+} would be preferred when applied along with therapeutic doses of ascorbate to destroy cancer cells due to the highest rate of catalysis of ascorbate oxidation with subsequent peroxide production. Equally active and more lipophilic MnPs, such as MnTnOct-2-PyP^{5+} and MnTnHexOE-2-PyP^{5+}, may be selected for the application in normal tissue oxidative stress related models as they are less efficacious in catalyzing ascorbate oxidation. However, much is still needed to fully understand therapeutic effects of redox-active drugs as they depend not only on their redox properties but on cellular and subcellular accumulation and colocalization with targeted species, many of those likely not yet identified.

Inhibition of Lipid Peroxidation by MnPs. Lipid peroxidation, i.e., the oxidative damage to polyunsaturated fatty acids, is initiated by the attack of reactive oxygen species, such as hydrogen peroxide, singlet oxygen, and hydroxyl radical.[124−126] This gives rise to lipid peroxyl, ROO$^\bullet$, and alkoxyl RO$^\bullet$ radicals and lipid hydroperoxides which propagate the lipid peroxidation. As most of the proteins are closely associated with membranes, the lipid peroxidation damages not only lipids but proteins also. Lipid peroxidation is involved in pathogenesis of a number of diseases such as cancer, atherosclerosis, diabetes, Alzheimer's disease, and Parkinson's disease, etc.[127−132] The peroxidation of arachidonic, linolenic, and docosahexanoic acids gives rise to malondialdehyde, MDA. MDA is also formed enzymatically during eicosanoid metabolism.[133] Due to the intrinsic aldehyde instability, the MDA is reactive toward DNA and amino acids, in particular lysine. HPLC-based thiobarbituric acid (TBA)-assay eliminates most of the interference that plagues the simple TBA assay and is therefore useful in screening the biological tissues on lipid peroxidation.[133] Figure 8 shows the magnitude of spontaneous lipid peroxidation affected by MnPs and measured as MDA with HPLC method. The data are expressed as percentage of peroxidation in control samples, which was taken as 100%.

The data in Figure 8 demonstrate a direct link between the $E_{1/2}$ of Mn^{III}P/Mn^{II}P and log $k_{cat}(O_2^{\bullet-})$, i.e., SOD-like activity, and the ability of MnPs to suppress lipid peroxidation. As $E_{1/2}$ parallels the log $k_{cat}(O_2^{\bullet-})$, it in turn correlates with the ability

dx.doi.org/10.1021/ic501329p | *Inorg. Chem.* 2014, 53, 11467−11483

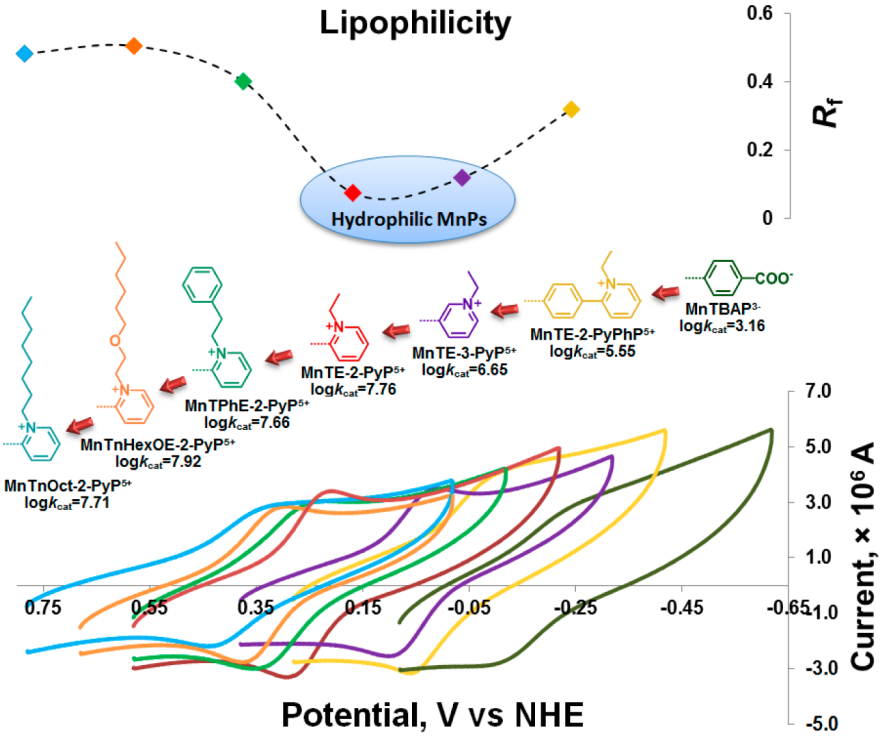

Figure 10. Schematic representations of the dominant properties of MnPs which control their therapeutic potential: $E_{1/2}$, log $k_{cat}(O_2^{\bullet-})$, and log P_{OW}. MnPs could be divided into 3 groups: (1) lipophilic and SOD-inactive [(of negative $E_{1/2}$ and log $k_{cat}(O_2^{\bullet-})$], the latter being lower than 5.7, situated in the right part of the figure, (2) lipophilic and SOD-active, situated in the left part of the figure, and (3) hydrophilic and SOD-active situated in the middle, i.e., in the minimum of the lipophilicity plot (Figure 5). Those MnPs that are lipophilic, SOD-active, and of positive $E_{1/2}$ are the most efficacious in *in vivo S. cerevisiae* assay and therefore bear the highest therapeutic potential.

of MnP to inhibit lipid peroxidation. Such a relationship [among the $E_{1/2}$, log $k_{cat}(O_2^{\bullet-})$, and inhibition of lipid peroxidation] is related to the electron deficiency of Mn site which controls ligand binding (in this case binding of lipid reactive species). See related discussion under Figure 6 and in the text in the Structure−Activity Relationships section.

MnTBAP^{3-}, with very negative $E_{1/2}$ = −194 mV vs NHE, did not suppress lipid peroxidation at up to 200 μM concentration. With less negative $E_{1/2}$ = −65 mV versus NHE, MnTE-2-PyPhP^{5+} fully suppressed the lipid peroxidation at ≥50 μM. Compounds with $E_{1/2}$ > +228 mV versus NHE were the most efficacious. Although MnTE-2-PyP^{5+} and MnTE-3-PyP^{5+} demonstrate similar superoxide scavenging ability in SOD-deficient *E. coli*[67] and *S. cerevisiae* assays, a clear difference between two of them was observed in lipid peroxidation assay. As cells are disrupted during preparation of brain homogenates, $E_{1/2}$ of MnPs, but not lipophilicity/bioavailability, gains controls over the magnitude of lipid peroxidation. At 1 μM concentration, MnTE-2-PyP^{5+} was very efficacious, whereas MnTE-3-PyP^{5+} did not inhibit lipid peroxidation. Despite similar $E_{1/2}$ values, the efficacy of larger molecule, MnTPhE-2-PyP^{5+}, was slightly lower relative to MnTE-2-PyP^{5+} and MnTnHexOE-2-PyP^{5+} (Figure 8A). This effect may be due to the steric hindrance toward lipid reactive species imposed by the bulkier substituents of MnTPhE-2-PyP^{5+} and MnTnHexOE-2-PyP^{5+} (Figure 8A). The oxygen-bearing MnTnHexOE-2-PyP^{5+} demonstrated higher potency than MnTnOct-2-PyP^{5+}. We have assigned this to the favorable interactions of polar oxygen atoms with lipid reactive species, guiding them toward Mn site. The impact of higher $E_{1/2}$ of MnTnOct-2-PyP^{5+} may not be excluded.

Effect of MnPs on the Aerobic Growth of SOD-Deficient *S. cerevisiae*. The aerobic growth of SOD-deficient *S. cerevisiae*, which lacks CuZnSOD, is an excellent *in vivo* model for the evaluation of the therapeutic potential of relatively lipophilic compounds within a class of water-soluble MnPs.[67] It is also $O_2^{\bullet-}$ specific *in vivo* model of oxidative stress.

The combined impact of $E_{1/2}$, lipophilicity, and bulkiness (size, shape) was demonstrated in yeast study. The most lipophilic compounds MnTnOct-2-PyP^{5+} and MnTnHexOE-2-PyP^{5+} are the most efficacious MnPs, presumably due to their higher accumulation in the cell and the higher $k_{cat}(O_2^{\bullet-})$ values relative to other MnPs. At 1−5 μM both compounds allow SOD-deficient yeast to grow as well as wild type (Figure 9). At higher concentrations both MnPs become toxic. The lipophilic, but bulkier, MnTPhE-2-PyP^{5+} has lower accumulation and is thus less efficient, but less toxic also. As seen before in *E. coli* assay,[2] the higher lipophilicity of MnTE-3-PyP^{5+} compensates for its lower $E_{1/2}$ and lower $k_{cat}(O_2^{\bullet-})$ and is thus equally efficacious as MnTE-2-PyP^{5+}. Both MnTE-3-PyP^{5+} and MnTE-2-PyP^{5+} become efficacious at concentrations above 5 μM. The compounds with very negative $E_{1/2}$ lacking SOD-like activity, MnTBAP^{3-} and MnTE-2-PyPhP^{5+}, are not protective to SOD-deficient *S. cerevisiae*.

■ CONCLUDING REMARKS

A series of MnPs with a wide range of metal-centered reduction potentials ($E_{1/2}$, from −190 to +340 mV vs NHE) and lipophilicities (log P_{OW}, from −7.67 to −1.67) have been synthesized and evaluated for their redox activities [$k_{cat}(O_2^{\bullet-})$, $k_{red}(ONOO^-)$, and v_0(HA$^-$ oxidation to A$^{\bullet-}$, ascorbyl radical)] and *in vitro* (lipid peroxidation) and *in vivo* therapeutic

dx.doi.org/10.1021/ic501329p | *Inorg. Chem.* 2014, 53, 11467−11483

potential (aerobic growth of SOD-deficient *S. cerevisiae*). Those porphyrins could be divided in 3 groups by their $E_{1/2}$ [which parallels log k_{cat} ($O_2^{\bullet-}$)] and lipophilicity as shown in Figure 10.

Two of those groups contain MnPs which are similarly lipophilic, yet in one group are the MnPs with negative $E_{1/2}$ and in the other with positive $E_{1/2}$. MnPs with negative $E_{1/2}$, despite high bioavailability, were inferior or nonefficacious in both *in vitro* and *in vivo* assays. MnPs with positive $E_{1/2}$ are the most efficacious ones. The third group comprises very hydrophilic *ortho* and *meta* MnTE-2-PyP^{5+} and MnTE-3-PyP^{5+} which are efficacious but several-fold less than lipophilic analogs of equal $E_{1/2}$. In summary our observations are the following: (1) The $E_{1/2}$ for the $Mn^{III}P/Mn^{II}P$ redox couple, dominated by the electron deficiency of porphyrin and its metal site, not only controls the ability of MnPs to eliminate $O_2^{\bullet-}$ and $ONOO^-$ but also the ability to prevent lipid peroxidation. The SOD-like activity appears to be proportional to the efficacy of MnP in preventing lipid peroxidation. The MnPs with highly positive $E_{1/2}$ (≥+228) and high SOD-like activity demonstrated strong inhibition of lipid peroxidation. MnTBAP^{3-} cannot inhibit lipid peroxidation, and MnTE-2-PyPhP^{5+} shows activity only at high concentration (≥50 μM). (2) The catalysis of ascorbate oxidation which involves reduction of $Mn^{III}P$ is controlled by the thermodynamics of $Mn^{III}P/Mn^{II}P$ redox couple. A bell shaped curve was observed for the MnP-driven catalysis of ascorbate oxidation with the highest $v_0(HA^-)$ observed at $E_{1/2}$ = +228 mV versus NHE (MnTE-2-PyP^{5+}). The data on ascorbate oxidation by MnP leading to a cytotoxic peroxide production (Figure 7) indicate the superiority of MnTE-2-PyP^{5+}, while the data on lipid peroxidation and *S. cerevisiae* suggest that lipophilic MnTnOct-2-PyP^{5+} and MnTnHexOE-2-PyP^{5+} may be superior as therapeutics. Hence, the latter compounds may be preferably applied in normal tissue injuries with oxidative stress background, whereas MnTE-2-PyP^{5+}, in combination with exogenous ascorbate, would be a therapeutic of choice for tumor treatment. (3) Only MnPs which disproportionate $O_2^{\bullet-}$ with a rate constant higher than the one for noncatalyzed, $O_2^{\bullet-}$ self-dismutation, i.e., log $k_{self\text{-}dismutation}(O_2^{\bullet-})$ = 5.70, mimic the SOD enzyme in protecting SOD-deficient yeast. MnTE-2-PyPhP^{5+} [log $k_{cat}(O_2^{\bullet-})$ = 5.55] or MnTBAP^{3-} [log $k_{cat}(O_2^{\bullet-})$ = 3.16] did not show any beneficial effect as they are not true SOD mimics. While $E_{1/2}$ controls the efficacy of MnPs in aqueous solution [i.e., log $k_{cat}(O_2^{\bullet-})$ and log $k_{red}(ONOO^-)$], the lipophilicity plays critical role *in vivo* also, as it governs the cellular and intracellular distribution of MnPs. Therefore, the compounds of somewhat lower SOD-like potency, such as MnTE-3-PyP^{5+}, still support the yeast growth as good as the MnTE-2-PyP^{5+} of higher log $k_{cat}(O_2^{\bullet-})$, as their cellular uptake is enhanced (Figure 9). (4) Enhanced toxicity of MnPs to SOD-deficient yeast is observed (Figure 9) with very lipophilic MnPs as they accumulate within a cell to higher levels and tend to localize in membranes disrupting their integrity. While fully protective in the region 1−5 μM, the MnTnOct-2-PyP^{5+} and MnTnHexOE-2-PyP^{5+} were already toxic at 20 μM. While MnTnHexOE-2-PyP^{5+} is a better inhibitor of lipid peroxidation, it is somewhat inferior to MnTnOct-2-PyP^{5+} in protecting *S. cerevisiae* which is likely due to the polar interactions between oxygen atoms and membrane structures. Jointly, high $k_{cat}(O_2^{\bullet-})$, high lipophilicity, and lower bulkiness contribute to the therapeutic potential of MnPs in *S. cerevisiae*. (5) We have originally developed MnPs as SOD mimics. Over the past decade we have shown that MnPs are involved in other actions, some of which may even predominate *in vivo*. Yet, thus far the experimental evidence (provided herein and elsewhere) indicates that the higher the SOD-like activity, the higher the therapeutic potential MnPs possess, even when reactions in question do not involve $O_2^{\bullet-}$ elimination. We can therefore safely conclude that the modification of a porphyrin molecule to enhance its SOD-like activity may still comprise the best experimental strategy in the design of redox-active drugs. (6) None of the data obtained here on MnTBAP^{3-} explain therapeutic effects reported elsewhere. Yet its *in vivo* efficacy justifies its future exploration. Its $ONOO^-$-related chemistry is ∼100-fold slower than that of Mn(III) *N*-substituted pyridylporphyrins (Table 4).[2] When compared to cationic pyridylporphyrins, MnTBAP^{3-} cannot be *in vivo* reduced to $Mn^{II}P$ by cellular reductants, such as ascorbate, in order to produce peroxide in subsequent reoxidation step (Figure 7). No reactivity toward lipid reactive species was observed (Figure 8). The lack of its SOD-like activity was proven here with SOD-deficient *S. cerevisiae* (Figure 9). It has insignificant catalase-like activity (Maia et al., submitted). Reactivity toward H_2O_2 may thus not play a major role in its actions. The role of reactive nitrogen species, other than $ONOO^-$, awaits further explorations.

■ ASSOCIATED CONTENT

Supporting Information

Additional figures and tables. This material is available free of charge via the Internet at http://pubs.acs.org.

■ AUTHOR INFORMATION

Corresponding Author

*E-mail: ibatinic@duke.edu. Phone: 919-684-2101.

Notes

The authors declare no competing financial interest.

■ ACKNOWLEDGMENTS

The authors acknowledge financial help from NIH U19AI067798 (A.T., I.S., I.B.-H.), and NIH/NCI Duke Comprehensive Cancer Center Core Grant (5-P30-CA14236-29) (I.S.). I.B.-H. and I.S. are consultants with BioMimetix Pharmaceutical, Inc. and Duke University and hold equities in BioMimetix Pharmaceutical Inc. L.B. acknowledges financial support from Kuwait University, Grant MB02/12, the excellent technical assistance of Milini Thomas, and Research Core Facility Grant SRUL02/13. R.G. acknowledges the financial support from State Committee of Science in Armenia (SCS 13-1D053) and ANSEF Biotech-3204. S.C. and R.R. acknowledge financial support from Centro de Biología Estructural del Mercosur (CeBEM), Programa de Desarrollo de Ciencias Básicas (PEDECIBA), and Agencia Nacional de Investigación e Innovación (ANII). R.R. was supported by grants from Universidad de la República and National Institutes of Health (RO1 AI095173). JS.R. and C.G.C.M. acknowledge CAPES and CNPq Research Councils.

■ REFERENCES

(1) Batinic-Haberle, I.; Benov, L.; Spasojevic, I.; Fridovich, I. *J. Biol. Chem.* **1998**, *273*, 24521−8.

(2) Batinic-Haberle, I.; Tovmasyan, A.; Roberts, E. R.; Vujaskovic, Z.; Leong, K. W.; Spasojevic, I. *Antioxid. Redox Signaling* **2014**, *20*, 2372−415.

(3) Batinic Haberle, I.; Tovmasyan, A.; Spasojevic, I. *BioInorg. React. Mech.* **2013**.

(4) Ferrer-Sueta, G.; Vitturi, D.; Batinic-Haberle, I.; Fridovich, I.; Goldstein, S.; Czapski, G.; Radi, R. *J. Biol. Chem.* **2003**, *278*, 27432−8.
(5) Ferrer-Sueta, G.; Batinic-Haberle, I.; Spasojevic, I.; Fridovich, I.; Radi, R. *Chem. Res. Toxicol.* **1999**, *12*, 442−9.
(6) Ferrer-Sueta, G.; Quijano, C.; Alvarez, B.; Radi, R. *Methods Enzymol.* **2002**, *349*, 23−37.
(7) Carballal, S.; Valez, V.; Batinic-Haberle, I.; Ferrer-Sueta, G.; Radi, R. *Free Radical Biol. Med.* **2013**, *65* (Supplement 2), S121−S122.
(8) Bloodsworth, A.; O'Donnell, V. B.; Batinic-Haberle, I.; Chumley, P. H.; Hurt, J. B.; Day, B. J.; Crow, J. P.; Freeman, B. A. *Free Radical Biol. Med.* **2000**, *28*, 1017−29.
(9) Trostchansky, A.; Ferrer-Sueta, G.; Batthyany, C.; Botti, H.; Batinic-Haberle, I.; Radi, R.; Rubbo, H. *Free Radical Biol. Med.* **2003**, *35*, 1293−300.
(10) Jaramillo, M. C.; Briehl, M. M.; Batinic Haberle, I.; Tome, M. E. *Free Radical Biol. Med.* **2013**, *65*, S25.
(11) Jaramillo, M. C.; Briehl, M. M.; Crapo, J. D.; Batinic-Haberle, I.; Tome, M. E. *Free Radical Biol. Med.* **2012**, *52*, 1272−84.
(12) Tovmasyan, A.; Weitner, T.; Jaramillo, M.; Wedmann, R.; Roberts, E.; Leong, K. W.; Filipovic, M.; Ivanovic-Burmazovic, I.; Benov, L.; Tome, M.; Batinic-Haberle, I. *Free Radical Biol. Med.* **2013**, *65*, S133.
(13) Batinić-Haberle, I.; Spasojević, I.; Stevens, R. D.; Hambright, P.; Fridovich, I. *J. Chem. Soc., Dalton Trans.* **2002**, 2689−2696.
(14) Spasojevic, I.; Miryala, S.; Tovmasyan, A.; Salvemini, D.; Vujaskovic, Z.; Batinic-Haberle, I.; St. Clair, D. *Free Radical Biol. Med.* **2011**, *51*, S98.
(15) Spasojevic, I.; Weitner, T.; Tovmasyan, A.; Sheng, H.; Miriyala, S.; Leu, D.; Rajic, Z.; Warner, D. S.; Clair, D. K.; Huang, T. T.; Batinic-Haberle, I. *Free Radical Biol. Med.* **2013**, *65*, S132.
(16) Rajic, Z.; Tovmasyan, A.; Spasojevic, I.; Sheng, H.; Lu, M.; Li, A. M.; Gralla, E. B.; Warner, D. S.; Benov, L.; Batinic-Haberle, I. *Free Radical Biol. Med.* **2012**, *52*, 1828−34.
(17) Batinic-Haberle, I.; Spasojevic, I. *Antioxid. Redox Signaling* **2014**, *20*, 2323−5.
(18) Aladag, M. A.; Turkoz, Y.; Sahna, E.; Parlakpinar, H.; Gul, M. *Acta Neurochir.* **2003**, *145*, 673−677.
(19) Bao, F.; DeWitt, D. S.; Prough, D. S.; Liu, D. *J. Neurosci Res.* **2003**, *71*, 220−7.
(20) Bao, F.; Liu, D. *Neuroscience* **2004**, *126*, 285−95.
(21) Cuzzocrea, S.; Costantino, G.; Mazzon, E.; De Sarro, A.; Caputi, A. P. *Br. J. Pharmacol.* **1999**, *128*, 1241−51.
(22) Hachmeister, J. E.; Valluru, L.; Bao, F.; Liu, D. *J. Neurotrauma* **2006**, *23*, 1766−78.
(23) Lee, B. I.; Chan, P. H.; Kim, G. W. *Stroke* **2005**, *36*, 2712−7.
(24) Leski, M. L.; Bao, F.; Wu, L.; Qian, H.; Sun, D.; Liu, D. *Free Radical Biol. Med.* **2001**, *30*, 613−24.
(25) Levrand, S.; Vannay-Bouchiche, C.; Pesse, B.; Pacher, P.; Feihl, F.; Waeber, B.; Liaudet, L. *Free Radical Biol. Med.* **2006**, *41*, 886−95.
(26) Ling, X.; Liu, D. *J. Neurosci. Res.* **2007**, *85*, 2175−85.
(27) Liu, D.; Bao, F.; Prough, D. S.; Dewitt, D. S. *J. Neurotrauma* **2005**, *22*, 1123−33.
(28) Liu, D.; Ling, X.; Wen, J.; Liu, J. *J. Neurochem.* **2000**, *75*, 2144−54.
(29) Liu, D.; Shan, Y.; Valluru, L.; Bao, F. *BMC Neurosci.* **2013**, *14*, 23.
(30) Loukili, N.; Rosenblatt-Velin, N.; Li, J.; Clerc, S.; Pacher, P.; Feihl, F.; Waeber, B.; Liaudet, L. *Cardiovasc. Res.* **2011**, *89*, 586−94.
(31) Luo, J.; Li, N.; Paul Robinson, J.; Shi, R. *J. Neurosci. Methods* **2002**, *120*, 105−12.
(32) Niwa, K.; Porter, V. A.; Kazama, K.; Cornfield, D.; Carlson, G. A.; Iadecola, C. *Am. J. Physiol.: Heart Circ. Physiol.* **2001**, *281*, H2417−24.
(33) Pan, H.; Shen, K.; Wang, X.; Meng, H.; Wang, C.; Jin, B. *PLoS One* **2014**, *9*, e86057.
(34) Patel, M.; Day, B. J.; Crapo, J. D.; Fridovich, I.; McNamara, J. O. *Neuron* **1996**, *16*, 345−55.
(35) Pires, K. M.; Ilkun, O.; Valente, M.; Boudina, S. *Obesity* **2014**, *22*, 178−87.
(36) Suresh, M. V.; Yu, B.; Lakshminrusimha, S.; Machado-Aranda, D.; Talarico, N.; Zeng, L.; Davidson, B. A.; Pennathur, S.; Raghavendran, K. *Surgery* **2013**, *154*, 980−90.
(37) Valluru, L.; Diao, Y.; Hachmeister, J. E.; Liu, D. *CNS Neurol. Disord.: Drug Targets* **2012**, *11*, 774−90.
(38) Wu, L.; Shan, Y.; Liu, D. *Cent. Nerv. Syst. Agents Med. Chem.* **2012**, *12*, 122−30.
(39) Yu, D.; Neeley, W. L.; Pritchard, C. D.; Slotkin, J. R.; Woodard, E. J.; Langer, R.; Teng, Y. D. *Stem Cells* **2009**, *27*, 1212−22.
(40) Cao, Y.; Fujii, M.; Ishihara, K.; Akiba, S.; Yasui, H.; Nabe, T. *Biol. Pharm. Bull.* **2013**, *36*, 850−5.
(41) Cui, Y. Y.; Qian, J. M.; Yao, A. H.; Ma, Z. Y.; Qian, X. F.; Zha, X. M.; Zhao, Y.; Ding, Q.; Zhao, J.; Wang, S.; Wu, J. *Transplantation* **2012**, *94*, 687−94.
(42) Li, Y.; Wende, A. R.; Nunthakungwan, O.; Huang, Y.; Hu, E.; Jin, H.; Boudina, S.; Abel, E. D.; Jalili, T. *FEBS J.* **2012**, *279*, 599−611.
(43) Aslan, M.; Ryan, T. M.; Adler, B.; Townes, T. M.; Parks, D. A.; Thompson, J. A.; Tousson, A.; Gladwin, M. T.; Patel, R. P.; Tarpey, M. M.; Batinic-Haberle, I.; White, C. R.; Freeman, B. A. *Proc. Natl. Acad. Sci. U.S.A.* **2001**, *98*, 15215−20.
(44) Batinic-Haberle, I.; Cuzzocrea, S.; Reboucas, J. S.; Ferrer-Sueta, G.; Mazzon, E.; Di Paola, R.; Radi, R.; Spasojevic, I.; Benov, L.; Salvemini, D. *Free Radical Biol. Med.* **2009**, *46*, 192−201.
(45) Benov, L.; Batinic-Haberle, I. *Free Radical Res.* **2005**, *39*, 81−8.
(46) Bottino, R.; Balamurugan, A. N.; Bertera, S.; Pietropaolo, M.; Trucco, M.; Piganelli, J. D. *Diabetes* **2002**, *51*, 2561−7.
(47) Bottino, R.; Balamurugan, A. N.; Tse, H.; Thirunavukkarasu, C.; Ge, X.; Profozich, J.; Milton, M.; Ziegenfuss, A.; Trucco, M.; Piganelli, J. D. *Diabetes* **2004**, *53*, 2559−68.
(48) Cernanec, J. M.; Weinberg, J. B.; Batinic-Haberle, I.; Guilak, F.; Fermor, B. *J. Rheumatol.* **2007**, *34*, 401−7.
(49) Chang, L. Y.; Subramaniam, M.; Yoder, B. A.; Day, B. J.; Ellison, M. C.; Sunday, M. E.; Crapo, J. D. *Am. J. Respir. Crit. Care Med.* **2003**, *167*, 57−64.
(50) Csont, T.; Viappiani, S.; Sawicka, J.; Slee, S.; Altarejos, J. Y.; Batinic-Haberle, I.; Schulz, R. *J. Mol. Cell. Cardiol.* **2005**, *39*, 833−40.
(51) Doyle, T.; Bryant, L.; Batinic-Haberle, I.; Little, J.; Cuzzocrea, S.; Masini, E.; Spasojevic, I.; Salvemini, D. *Neuroscience* **2009**, *164*, 702−10.
(52) Gauter-Fleckenstein, B.; Fleckenstein, K.; Owzar, K.; Jiang, C.; Batinic-Haberle, I.; Vujaskovic, Z. *Free Radical Biol. Med.* **2008**, *44*, 982−9.
(53) Gauter-Fleckenstein, B.; Fleckenstein, K.; Owzar, K.; Jiang, C.; Reboucas, J. S.; Batinic-Haberle, I.; Vujaskovic, Z. *Free Radical Biol. Med.* **2010**, *48*, 1034−43.
(54) Jackson, I. L.; Gaunter-Fleckenstein, B. M.; Batinic-Haberle, I.; Poulton, S.; Zhao, Y.; Dewhirst, M. W.;Vujaskovic, Z. *24th Annual Meeting of the European Society for Hyperthermic Oncology*; 2007.
(55) Jaramillo, M. C.; Frye, J. B.; Crapo, J. D.; Briehl, M. M.; Tome, M. E. *Cancer Res.* **2009**, *69*, 5450−7.
(56) Li, H.; Wang, Y.; Pazhanisamy, S. K.; Shao, L.; Batinic-Haberle, I.; Meng, A.; Zhou, D. *Free Radical Biol. Med.* **2011**, *51*, 30−7.
(57) Lubbers, N. L.; Polakowski, J. S.; Crapo, J. D.; Wegner, C. D.; Cox, B. F. *J. Cardiovasc. Pharmacol.* **2003**, *41*, 714−9.
(58) Mackensen, G. B.; Patel, M.; Sheng, H.; Calvi, C. L.; Batinic-Haberle, I.; Day, B. J.; Liang, L. P.; Fridovich, I.; Crapo, J. D.; Pearlstein, R. D.; Warner, D. S. *J. Neurosci.* **2001**, *21*, 4582−92.
(59) Makinde, A. Y.; Luo-Owen, X.; Rizvi, A.; Crapo, J. D.; Pearlstein, R. D.; Slater, J. M.; Gridley, D. S. *Anticancer Res.* **2009**, *29*, 107−18.
(60) Makinde, A. Y.; Rizvi, A.; Crapo, J. D.; Pearlstein, R. D.; Slater, J. M.; Gridley, D. S. *Radiat. Res.* **2010**, *173*, 441−52.
(61) Moeller, B. J.; Cao, Y.; Li, C. Y.; Dewhirst, M. W. *Cancer Cell* **2004**, *5*, 429−41.
(62) Nin, N.; Cassina, A.; Boggia, J.; Alfonso, E.; Botti, H.; Peluffo, G.; Trostchansky, A.; Batthyany, C.; Radi, R.; Rubbo, H.; Hurtado, F. J. *Intensive Care Med.* **2004**, *30*, 2271−8.
(63) Pazhanisamy, S. K.; Li, H.; Wang, Y.; Batinic-Haberle, I.; Zhou, D. *Mutagenesis* **2011**, *26*, 431−5.

(64) Piganelli, J. D.; Flores, S. C.; Cruz, C.; Koepp, J.; Batinic-Haberle, I.; Crapo, J.; Day, B.; Kachadourian, R.; Young, R.; Bradley, B.; Haskins, K. *Diabetes* **2002**, *51*, 347−55.
(65) Rabbani, Z. N.; Spasojevic, I.; Zhang, X.; Moeller, B. J.; Haberle, S.; Vasquez-Vivar, J.; Dewhirst, M. W.; Vujaskovic, Z.; Batinic-Haberle, I. *Free Radical Biol. Med.* **2009**, *47*, 992−1004.
(66) Sompol, P.; Ittarat, W.; Tangpong, J.; Chen, Y.; Doubinskaia, I.; Batinic-Haberle, I.; Abdul, H. M.; Butterfield, D. A.; St. Clair, D. K. *Neuroscience* **2008**, *153*, 120−30.
(67) Tovmasyan, A.; Reboucas, J. S.; Benov, L. *Antioxid. Redox Signaling* **2014**, *20*, 2416−36.
(68) Zhao, Y.; Chaiswing, L.; Oberley, T. D.; Batinic-Haberle, I.; St. Clair, W.; Epstein, C. J.; St. Clair, D. *Cancer Res.* **2005**, *65*, 1401−5.
(69) Reboucas, J. S.; Spasojevic, I.; Batinic-Haberle, I. *J. Biol. Inorg. Chem.* **2008**, *13*, 289−302.
(70) Day, B. J.; Fridovich, I.; Crapo, J. D. *Arch. Biochem. Biophys.* **1997**, *347*, 256−62.
(71) Álvarez, L.; Suarez, S.; Bikiel, D.; Reboucas, J.; Batinić-Haberle, I.; Martí, M.; Doctorovich, F. *Inorg. Chem.* **2014**, submitted.
(72) Celic, T.; Španjol, J.; Bobinac, M.; Tovmasyan, A.; Reboucas, J. S.; Batinic Haberle, I.; Bobinac, D. *Free Radical Res.* **2014**, DOI: 10.3109/10715762.2014.960865.
(73) Reboucas, J. S.; Spasojevic, I.; Batinic-Haberle, I. *J. Pharm. Biomed. Anal.* **2008**, *48*, 1046−9.
(74) Hitomi, Y.; Ekawa, T.; Kodera, M. *Chem. Lett.* **2014**, *43*, 732−734.
(75) Reboucas, J. S.; DeFreitas-Silva, G.; Spasojevic, I.; Idemori, Y. M.; Benov, L.; Batinic-Haberle, I. *Free Radical Biol. Med.* **2008**, *45*, 201−10.
(76) Batinić-Haberle, I.; Spasojević, I.; Hambright, P.; Benov, L.; Crumbliss, A. L.; Fridovich, I. *Inorg. Chem.* **1999**, *38*, 4011−4022.
(77) Evans, M. K.; Tovmasyan, A.; Batinic-Haberle, I.; Devi, G. R. *Free Radical Biol. Med.* **2014**, *68*, 302−14.
(78) Ye, X.; Fels, D.; Tovmasyan, A.; Aird, K. M.; Dedeugd, C.; Allensworth, J. L.; Kos, I.; Park, W.; Spasojevic, I.; Devi, G. R.; Dewhirst, M. W.; Leong, K. W.; Batinic-Haberle, I. *Free Radical Res.* **2011**, *45*, 1289−306.
(79) Batinic-Haberle, I.; Reboucas, J. S.; Benov, L.; Spasojevic, I. Chemistry, biology and medical effects of water soluble metalloporphyrins. In *Handbook of Porphyrin Science*; Kadish, K. M., Smith, K. M., Guillard, R., Eds.; World Scientific: Singapore, 2011; Vol. *11*; pp 291−393.
(80) Tovmasyan, A. G.; Rajic, Z.; Spasojevic, I.; Reboucas, J. S.; Chen, X.; Salvemini, D.; Sheng, H.; Warner, D. S.; Benov, L.; Batinic-Haberle, I. *Dalton Trans.* **2011**, *40*, 4111−21.
(81) Kos, I.; Reboucas, J. S.; DeFreitas-Silva, G.; Salvemini, D.; Vujaskovic, Z.; Dewhirst, M. W.; Spasojevic, I.; Batinic-Haberle, I. *Free Radical Biol. Med.* **2009**, *47*, 72−8.
(82) Engelmann, F. M.; Rocha, S. V.; Toma, H. E.; Araki, K.; Baptista, M. S. *Int. J. Pharm.* **2007**, *329*, 12−8.
(83) Miriyala, S.; Spasojevic, I.; Tovmasyan, A.; Salvemini, D.; Vujaskovic, Z.; St Clair, D.; Batinic-Haberle, I. *Biochim. Biophys. Acta* **2012**, *1822*, 794−814.
(84) Spasojevic, I.; Batinic-Haberle, I.; Stevens, R. D.; Hambright, P.; Thorpe, A. N.; Grodkowski, J.; Neta, P.; Fridovich, I. *Inorg. Chem.* **2001**, *40*, 726−39.
(85) Batinic-Haberle, I.; Reboucas, J. S.; Spasojevic, I. *Antioxid. Redox Signaling* **2010**, *13*, 877−918.
(86) Eckshtain, M.; Zilbermann, I.; Mahammed, A.; Saltsman, I.; Okun, Z.; Maimon, E.; Cohen, H.; Meyerstein, D.; Gross, Z. *Dalton Trans* **2009**, 7879−82.
(87) Lee, J. B.; Hunt, J. A.; Groves, J. T. *J. Am. Chem. Soc.* **1998**, *120*, 7493−7501.
(88) Lee, J. B.; Hunt, J. A.; Groves, J. T. *J. Am. Chem. Soc.* **1998**, *120*, 6053−6061.
(89) Buege, J. A.; Aust, S. D. *Methods Enzymol.* **1978**, *52*, 302−10.
(90) Ali, D. K.; Oriowo, M.; Tovmasyan, A.; Batinic-Haberle, I.; Benov, L. *Redox Biol.* **2013**, *1*, 457−66.
(91) Gralla, E. B.; Valentine, J. S. *J. Bacteriol.* **1991**, *173*, 5918−20.
(92) Kaiser, C.; Michaelis, S.; Mitchell, A. *Methods in Yeast Genetics*; Cold Spring Harbor Laboratory Press: Cold Spring Harbor, NY, 1994.
(93) Tovmasyan, A.; Weitner, T.; Sheng, H.; Lu, M.; Rajic, Z.; Warner, D. S.; Spasojevic, I.; Reboucas, J. S.; Benov, L.; Batinic-Haberle, I. *Inorg. Chem.* **2013**, *52*, 5677−91.
(94) Tovmasyan, A.; Sheng, H.; Weitner, T.; Arulpragasam, A.; Lu, M.; Warner, D. S.; Vujaskovic, Z.; Spasojevic, I.; Batinic-Haberle, I. *Med. Princ. Pract.* **2013**, *22*, 103−30.
(95) Holley, A. K.; Xu, Y.; Noel, T.; Bakthavatchalu, V.; Batinic-Haberle, I.; St. Clair, D. K. *Antioxid. Redox Signaling* **2014**, 2347−2360.
(96) Miriyala, S.; Holley, A. K.; St. Clair, D. K. *Anti-Cancer Agents Med. Chem.* **2011**, *11*, 181−90.
(97) Zhao, Y.; Miriyala, S.; Miao, L.; Mitov, M.; Schnell, D.; Dhar, S. K.; Cai, J.; Klein, J. B.; Sultana, R.; Butterfield, D. A.; Vore, M.; Batinic-Haberle, I.; Bondada, S.; St. Clair, D. K. *Free Radical Biol. Med.* **2014**, *72*, 55−65.
(98) Ellerby, R. M.; Cabelli, D. E.; Graden, J. A.; Valentine, J. S. *J. Am. Chem. Soc.* **1996**, *118*, 6556−61.
(99) Klug-Roth, D.; Fridovich, I.; Rabani, J. *J. Am. Chem. Soc.* **1973**, *95*, 2786−90.
(100) Vance, C. K.; Miller, A. F. *J. Am. Chem. Soc.* **1998**, *120*, 461−467.
(101) Batinic-Haberle, I.; Spasojevic, I.; Stevens, R. D.; Hambright, P.; Neta, P.; Okado-Matsumoto, A.; Fridovich, I. *Dalton Trans.* **2004**, 1696−702.
(102) Coulter, E. D.; Emerson, J. P.; Kurtz, D. M.; Cabelli, D. E. *J. Am. Chem. Soc.* **2000**, *122*, 11555−11556.
(103) Chen, S.-M.; Sun, P.-J.; Su, Y. O. *J. Electroanal. Chem. Interfacial Electrochem.* **1990**, *294*, 151−64.
(104) Rodgers, K. R.; Reed, R. A.; Su, Y. O.; Spiro, T. G. *Inorg. Chem.* **1992**, *31*, 2688−2700.
(105) Carnieri, N.; Harriman, A.; Porter, G. *J. Chem. Soc., Dalton Trans.* **1982**, 931−8.
(106) Boucher, L. J. *Coord. Chem. Rev.* **1972**, *7*, 289−329.
(107) Jin, N.; Groves, J. T. *J. Am. Chem. Soc.* **1999**, *121*, 2923−2924.
(108) Harriman, A. *J. Chem. Soc., Dalton Trans.* **1984**, 141−146.
(109) Harriman, A.; Porter, G. *J. Chem. Soc., Faraday Trans 2* **1979**, *75*, 1543−1552.
(110) Liu, M.-h.; Su, Y. O. *J. Electroanal. Chem.* **1997**, *426*, 197−203.
(111) Lahaye, D.; Groves, J. T. *J. Inorg. Biochem* **2007**, *101*, 1786−97.
(112) Weitner, T.; Kos, I.; Mandic, Z.; Batinic-Haberle, I.; Birus, M. *Dalton Trans.* **2013**, *42*, 14757−65.
(113) Faulkner, K. M.; Liochev, S. I.; Fridovich, I. *J. Biol. Chem.* **1994**, *269*, 23471−6.
(114) Weitzel, D. H.; Tovmasyan, A.; Ashcraft, K. A.; Rajic, Z.; Weitner, T.; Liu, C.; Li, W.; Buckley, A. F.; Prasad, M. R.; Young, K. H.; Rodriguiz, R. M.; Wetsel, W. C.; Peters, K. B.; Spasojevic, I.; Herndon, J. I., II; Batinic-Haberle, I.; Dewhirst, M. W. *Mol. Cancer Ther.* **2014**, DOI: 10.1158/1535-7163.MCT-14-0343.
(115) Jaramillo, M. C.; Briehl, M. M.; Tome, M. E. *Free Radical Biol. Med.* **2010**, *49*, S63.
(116) Gao, M. C.; Jia, X. D.; Wu, Q. F.; Cheng, Y.; Chen, F. R.; Zhang, J. *Acta Pharmacol. Sin.* **2011**, *32*, 528−36.
(117) Nonn, L.; Berggren, M.; Powis, G. *Mol. Cancer Res.* **2003**, *1*, 682−9.
(118) Sampson, N.; Koziel, R.; Zenzmaier, C.; Bubendorf, L.; Plas, E.; Jansen-Durr, P.; Berger, P. *Mol. Endocrinol.* **2011**, *25*, 503−15.
(119) Shen, K. K.; Ji, L. L.; Chen, Y.; Yu, Q. M.; Wang, Z. T. *Biosci. Trends* **2011**, *5*, 30−7.
(120) Sorokina, L. V.; Solyanik, G. I.; Pyatchanina, T. V. *Exp. Oncol.* **2010**, *32*, 249−53.
(121) Hempel, N.; Carrico, P. M.; Melendez, J. A. *Anti-Cancer Agents Med. Chem.* **2011**, *11*, 191−201.
(122) Ashcraft, K. A.; Palmer, G.; Spasojevic, I.; Batinic-Haberle, I.; Dewhirst, M. W. *58th Annual Meeting of the Radiation Research Society*; 2012; 129.
(123) Yulyana, Y.; Tovmasyan, A.; Ho, I. A. W.; Sia, K. C.; P, N. J.; H, N. W.; Guo, C. M.; Hui, K. M.; Batinic-Haberle, I.; Lam, P. *Free Radical Res.* **2014**, in revision.

(124) Adibhatla, R. M.; Hatcher, J. F. *Antioxid. Redox Signaling* **2010**, *12*, 125−169.
(125) Niki, E.; Yoshida, Y.; Saito, Y.; Noguchi, N. *Biochem. Biophys. Res. Commun.* **2005**, *338*, 668−76.
(126) Yin, H.; Xu, L.; Porter, N. A. *Chem. Rev.* **2011**, *111*, 5944−72.
(127) Berliner, J. A.; Heinecke, J. W. *Free Radical Biol. Med.* **1996**, *20*, 707−27.
(128) Hammad, L. A.; Wu, G.; Saleh, M. M.; Klouckova, I.; Dobrolecki, L. E.; Hickey, R. J.; Schnaper, L.; Novotny, M. V.; Mechref, Y. *Rapid Commun. Mass Spectrom.* **2009**, *23*, 863−76.
(129) Wu, R. P.; Hayashi, T.; Cottam, H. B.; Jin, G.; Yao, S.; Wu, C. C.; Rosenbach, M. D.; Corr, M.; Schwab, R. B.; Carson, D. A. *Proc. Natl. Acad. Sci. U.S.A.* **2010**, *107*, 7479−84.
(130) Silverstein, R. L.; Febbraio, M. *Sci. Signaling* **2009**, *2*, re3.
(131) Montine, T. J.; Montine, K. S.; McMahan, W.; Markesbery, W. R.; Quinn, J. F.; Morrow, J. D. *Antioxid. Redox Signaling* **2005**, *7*, 269−75.
(132) Porter, F. D.; Scherrer, D. E.; Lanier, M. H.; Langmade, S. J.; Molugu, V.; Gale, S. E.; Olzeski, D.; Sidhu, R.; Dietzen, D. J.; Fu, R.; Wassif, C. A.; Yanjanin, N. M.; Marso, S. P.; House, J.; Vite, C.; Schaffer, J. E.; Ory, D. S. *Sci. Transl. Med.* **2010**, *2*, 56ra81.
(133) Halliwell, B.; Gutteridge, J. M. C. *Free Radicals in Biology and Medicine*; Oxford University Press: New York, 2007.